The Plant Cell, Vol. 26: 497–515, January 2014, www.plantcell.org

The Rice TAL Effector–Dependent Resistance Protein XA10 Triggers Cell Death and Calcium Depletion in the Endoplasmic Reticulum[W]

Dongsheng Tian,[a,1] Junxia Wang,[a,1] Xuan Zeng,[a,b,1] Keyu Gu,[a,1] Chengxiang Qiu,[a] Xiaobei Yang,[a] Zhiyun Zhou,[a] Meiling Goh,[a] Yanchang Luo,[a] Maki Murata-Hori,[a] Frank F. White,[c] and Zhongchao Yin[a,b,2]

[a] Temasek Life Sciences Laboratory, National University of Singapore, Singapore 117604, Republic of Singapore
[b] Department of Biological Sciences, National University of Singapore, Singapore 117543, Republic of Singapore
[c] Department of Plant Pathology, Kansas State University, Manhattan, Kansas 66506

The recognition between disease resistance (*R*) genes in plants and their cognate avirulence (*Avr*) genes in pathogens can produce a hypersensitive response of localized programmed cell death. However, our knowledge of the early signaling events of the *R* gene–mediated hypersensitive response in plants remains limited. Here, we report the cloning and characterization of *Xa10*, a transcription activator–like (TAL) effector-dependent *R* gene for resistance to bacterial blight in rice (*Oryza sativa*). *Xa10* contains a binding element for the TAL effector AvrXa10 ($EBE_{AvrXa10}$) in its promoter, and AvrXa10 specifically induces *Xa10* expression. Expression of *Xa10* induces programmed cell death in rice, *Nicotiana benthamiana*, and mammalian HeLa cells. The *Xa10* gene product XA10 localizes as hexamers in the endoplasmic reticulum (ER) and is associated with ER Ca^{2+} depletion in plant and HeLa cells. XA10 variants that abolish programmed cell death and ER Ca^{2+} depletion in *N. benthamiana* and HeLa cells also abolish disease resistance in rice. We propose that XA10 is an inducible, intrinsic terminator protein that triggers programmed cell death by a conserved mechanism involving disruption of the ER and cellular Ca^{2+} homeostasis.

INTRODUCTION

The hypersensitive response (HR) of plants is a form of programmed cell death (PCD) that commonly occurs during disease resistance (*R*) gene–mediated resistance to a pathogen that carries a corresponding avirulence (*Avr*) gene (Heath, 2000). The HR occurs at the site of attempted pathogen invasion and, in concert with accompanied defense responses, restricts the growth of pathogens to the infection site (Heath, 2000). Many *R* genes, upon perception of an avirulent pathogen, trigger an HR by a mechanism involving cellular efflux of anions and potassium and influx of calcium and hydrogen ions (Grant et al., 2000). Following the ion flux, the affected cells generate an oxidative burst, producing reactive oxygen species (ROS) (Levine et al., 1994). The ROS cause lipid peroxidation and oxidative damage to DNA and proteins, resulting in PCD and the formation of local lesions (Montillet et al., 2005). The ROS burst also drives cross-linking of cell wall compounds and leads to expression of plant genes involved in cellular protection and defense (Bradley et al., 1992; Jabs et al., 1997). A broad range of *R* genes have been identified. However, our understanding of the early signaling events of *R* gene–mediated HR in plants remains limited (Ma and Berkowitz, 2007).

Bacterial blight of rice (*Oryza sativa*), caused by *Xanthomonas oryzae* pv *oryzae*, is an important disease throughout the major rice growing regions of the world. During infection, *X. oryzae* pv *oryzae* strains deliver members of the large AvrBs3-related effector family into host cells via the bacterial type III secretion system (Yang and White, 2004). AvrBs3-like effectors, also referred to as transcription activator–like (TAL) effectors (Yang et al., 2006), function as transcription factors and induce expression of specific host genes within the host cells (Gu et al., 2005; Yang et al., 2006; Kay et al., 2007; Römer et al., 2007; Sugio et al., 2007; Strauss et al., 2012). TAL effector–mediated host gene induction is determined by the repetitive central region of each effector, which consists of near-perfect direct repeats of 33– to 35–amino acid residues. The repetitive region determines the sequence specificity of the targeted DNA elements within the promoters of the affected genes (Boch et al., 2009). Strains of *Xanthomonas* use TAL effectors to induce host susceptibility (*S*) genes, which facilitate bacterial infection and promote diseases (Yang et al., 2006; Kay et al., 2007; Sugio et al., 2007; Antony et al., 2010). Rice and pepper (*Capsicum annuum*) have evolved mechanisms of self-immolation by the adaptation of TAL effector–specific *R* genes (Gu et al., 2005; Römer et al., 2007). Individual TAL effectors can have dual functions in regulating host gene expression, serving as important virulence factors to induce *S* gene expression for susceptibility and serving as important factors triggering resistance in cultivars with cognate *R* genes (Kay et al., 2007; Römer et al., 2007; Antony et al., 2010).

Positional cloning and RNA sequencing approaches have identified three *R* genes whose expression is modulated by TAL effectors, *Xa27*, *Bs3*, and *Bs4C-R* (Gu et al., 2005; Kay et al., 2007; Strauss et al., 2012). The products of the TAL effector–dependent

[1] These authors contributed equally to this work.
[2] Address correspondence to yinzc@tll.org.sg.
The author responsible for distribution of materials integral to the findings presented in this article in accordance with the policy described in the Instructions for Authors (www.plantcell.org) is: Zhongchao Yin (yinzc@tll.org.sg).
[W] Online version contains Web-only data.
www.plantcell.org/cgi/doi/10.1105/tpc.113.119255

R genes show no apparent sequence similarities. *Xa27* encodes a small protein that localizes to the apoplast of rice cells and *Xa27* expression strictly depends on the cognate TAL effector AvrXa27 (Gu et al., 2005). *Xa27* elicits an HR in rice (Gu et al., 2005). The pepper *R* gene *Bs3* confers resistance to strains of *Xanthomonas campestris* pv *vesicatoria* containing the TAL effector gene *avrBs3* and encodes a product homologous to flavin-dependent monooxygenases, indicating that BS3 may have an enzymatic function (Römer et al., 2007). The pepper *R* gene *Bs4C-R* confers resistance to *X. campestris* pv *vesicatoria*, and the TAL effector AvrBs4 induces *Bs4C-R* expression. *Bs4C-R* encodes a putative 164–amino acid protein that shares no significant sequence similarity to any protein of known function (Strauss et al., 2012). Another dominant *R* gene, tomato (*Solanum lycopersicum*) *Bs4*, triggers resistance to *X. campestris* pv *vesicatoria* in response to the TAL effector AvrBs4 (Schornack et al., 2004). However, the *Bs4* product BS4 appears to perceive AvrBs4 by a different mechanism from TAL effector–mediated induction, as *Bs4*-mediated recognition does not require the C-terminal nuclear localization signal motifs (Ballvora et al., 2001). Therefore, BS4 more likely functions in a manner similar to the many nucleotide binding site–leucine-rich repeat–type R proteins of which BS4 is a member (Yue et al., 2012).

Originally identified from rice cultivar Cas 209, the *R* gene *Xa10* confers race-specific resistance to rice bacterial blight (Yoshimura et al., 1983). The cognate *Avr* gene *avrXa10* of *X. oryzae* pv *oryzae* strain PXO86 encodes a TAL effector containing 15.5 repeats (Hopkins et al., 1992). The interaction of *avrXa10* and *Xa10* triggers a strong HR characterized by very short disease lesions on *Xa10* plants and provides resistance at all developmental stages (Gu et al., 2008). We previously mapped the *Xa10* gene to the long arm of chromosome 11 of rice in a 0.28-centimorgan region between proximal marker M491 and distal marker M419 and cosegregating with markers S723 and M604 (Gu et al., 2008). Here, we report the isolation and characterization of the *Xa10* gene and XA10 protein.

RESULTS

Map-Based Cloning of *Xa10*

The *Xa10* locus in rice cultivar IRBB10A is flanked by markers M491 and M419 and cosegregated with marker S723 (Gu et al., 2008). M491 and S723 were used to screen a *Xa10* BAC library constructed from the rice line IRBB10A containing *Xa10*. BAC clone 44M10 was selected on the basis of the presence of both markers (Figure 1A). The insert in 44M10 was sequenced, and 44M10-derived subclones were used for transformation of susceptible cultivar Nipponbare. Six of the nine 44M10 subclones, including the smallest subclone PX3834 encompassing 3834 bp, produced transgenic plants that were resistant to *X. oryzae* pv *oryzae* strain PXO99^{A}(*avrXa10*) (Figure 1A; Supplemental Table 1). The T1 progeny of the resistant transgenic lines derived from PX3834 and other larger functional subclones maintained the AvrXa10-dependent resistance phenotype, conferring resistance to PXO99^{A}(*avrXa10*), while showing moderate or complete susceptibility to PXO99^{A} (Figure 1B; Supplemental Table 2).

We identified only one *Xa10* candidate open reading frame within the 3834-bp region of PX3834. A 563-bp cDNA of *Xa10* was isolated from inoculated tissues of IRBB10A by RT-PCR and rapid amplification of cDNA ends (RACE). The *Xa10* genomic region contains a 249-bp intron in the 3′ untranslated region in comparison to the cDNA clone (Figure 1C). DNA gel blot analysis revealed that *Xa10* is present in IRBB10 and IRBB10A but not in the four susceptible rice cultivars tested (Supplemental Figure 1). *Xa10* encodes a small novel protein consisting of 126–amino acid residues, which is predicted to have four potential transmembrane helices (M1 to M4), among which, M2 contains charged amino acid residues (Figure 1D; Supplemental Figure 2). XA10 carries a series of acidic amino acid residues at position 118 to 122 (ED motif) in the C-terminal region (Figure 1D). Putative paralogs/orthologs of XA10 were identified in cultivar Nipponbare (National Center for Biotechnology Information accession numbers ABA94452 and ABA94457) as well as in three wild rice species (CW524693, CZ142765, and CZ853552) (Supplemental Figure 3). None of the putative paralogs/orthologs have been assigned a function.

AvrXa10 Specifically Targets to $EBE_{AvrXa10}$ for *Xa10* Induction

The expression of *Xa10* in cultivar IRBB10A was induced upon inoculation with PXO99^{A} (*avrXa10*) (Figures 2A and 2B). The *Xa10* transcripts were detected as early as 3 h after inoculation, peaked at 6 to 12 h after inoculation, and remained detectable at 48 h after inoculation (Figures 2A and 2B). No *Xa10* transcripts were detected in mock inoculations with water or with strains of PXO99^{A} either lacking *avrXa10* or containing *avrXa10* derivatives with mutations in the nuclear localization signals or deletion in the acidic transcriptional activation domain (Figures 2C and 2D). AvrXa10-dependent induction was also observed for the *Xa10* transgene in transgenic line L198 carrying genomic clone SA4671 (Supplemental Figure 4). The recessive rice *R* gene *xa5*, which confers disease resistance to *xa5*-incompatible *X. oryzae* pv *oryzae* strains (Iyer and McCouch, 2004), greatly attenuates TAL effector–mediated induction of the *R* gene *Xa27* by the cognate TAL effector AvrXa27 (Gu et al., 2009). Both AvrXa10-dependent *Xa10* induction and the *Xa10*-mediated resistance to PXO99^{A}(*avrXa10*) were partially suppressed in *xa5* and *Xa10* double homozygous plants (DH) (Figures 2E and 2F; Supplemental Figure 5).

The AvrXa10-dependent *Xa10* promoter activity was assayed with a β-glucuronidase (GUS) reporter system (Supplemental Figure 6) and transient expression in *Nicotiana benthamiana*. The *Xa10* promoter, consisting of nucleotides from positions −220 to −1 ($P_{Xa10\text{-}220}$) relative to the transcription start site, was found to retain AvrXa10-dependent promoter activity (Figures 2G and 2I; Supplemental Figure 6). A putative effector binding element (EBE) for AvrXa10 ($EBE_{AvrXa10}$) was identified in $P_{Xa10\text{-}220}$ based on the consensus of DNA binding specificity for TAL effectors (Figures 2G and 2H). The GUS reporter construct harboring only $EBE_{AvrXa10}$ displayed similar AvrXa10-dependent promoter activity to that of $P_{Xa10\text{-}220}$ (Figure 2I). As a control, $EBE_{AvrXa10}$ did not show AvrXa27-dependent promoter activity (Figure 2J). Conversely, a GUS reporter construct with $EBE_{AvrXa27}$ exhibited AvrXa27-dependent expression, but not AvrXa10-dependent expression (Figure 2J). Electrophoretic mobility shift assays demonstrated

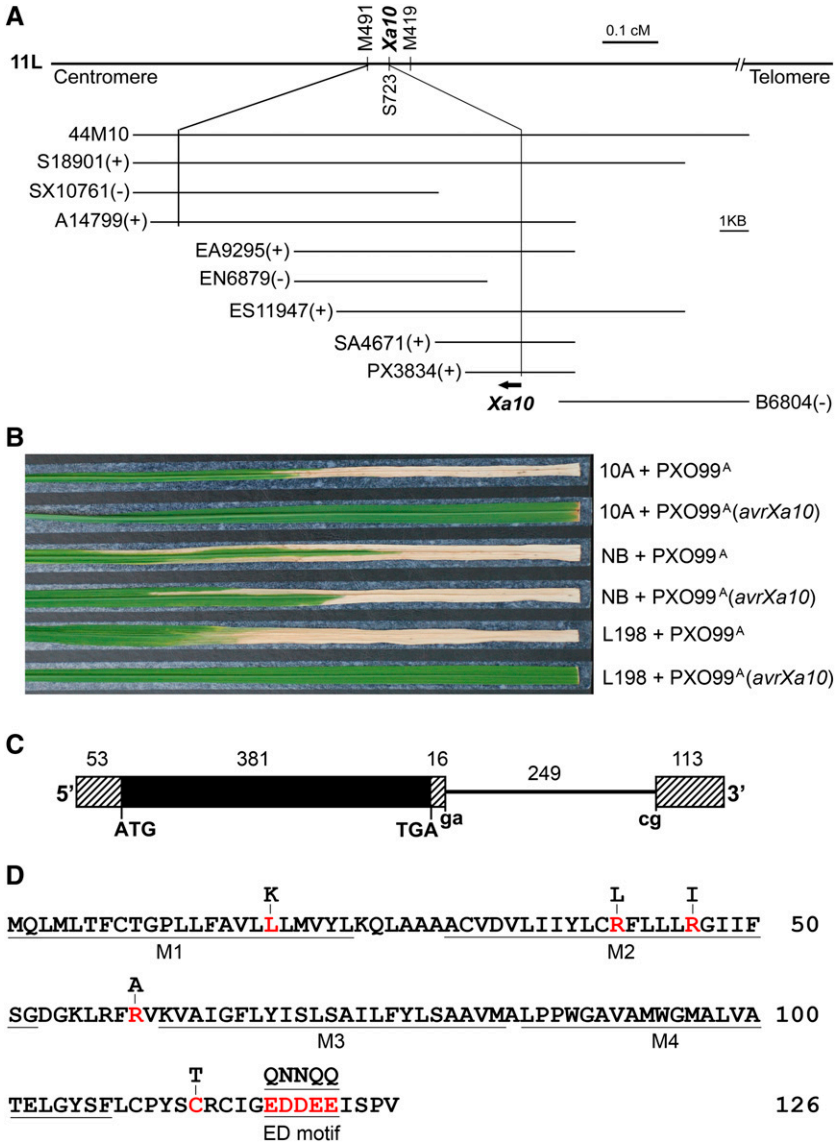

Figure 1. Map-Based Cloning of the *Xa10* Gene.

(A) Genetic and physical maps of the *Xa10* locus. The *Xa10* locus is flanked by molecular markers M491 and M419 and cosegregated with S723 (Gu et al., 2008). BAC clone 44M10 was identified by markers M491 and S723. The 44M10 subclones that produced bacterial blight–resistant transgenic plants are marked with "+;" otherwise, they are marked with "−." Vertical lines link the genetic locations of M491 and the *Xa10* locus to their positions on the physical map. The position of the *Xa10* gene is indicated with short bold line with arrowhead pointing to the direction of transcription. cM, centimorgans.

(B) Disease phenotype of rice lines 2 weeks after inoculation with *X. oryzae* pv *oryzae* strains PXO99^{A} or PXO99^{A}(*avrXa10*). 10A, IRBB10A; NB, Nipponbare; L198, *Xa10* transgenic line L198 carrying the *Xa10* genomic clone SA4671.

(C) Gene structure of *Xa10*. The schematic map shows the coding region (closed box), the 5′ and 3′ untranslated regions (hatched boxes), and the intron in the 3′ untranslated region of the *Xa10* gene (line). The 5′ and 3′ splice junctions (ga and cg) of the intron are indicated. The numbers indicate the size of each substructure.

(D) The deduced amino acid sequence of XA10. The transmembrane helices (M1 to M4) and the acidic ED motif in the C-terminal region of XA10 are underlined. Amino acid residues and the ED motif which were used to generate XA10 variants are displayed in red letters. Mutated amino acid residues are shown above the corresponding amino acid residue positions. Transmembrane helices were predicted using the SOSUI program (http://bp.nuap.nagoya-u.ac.jp/sosui/sosui_submit.html).

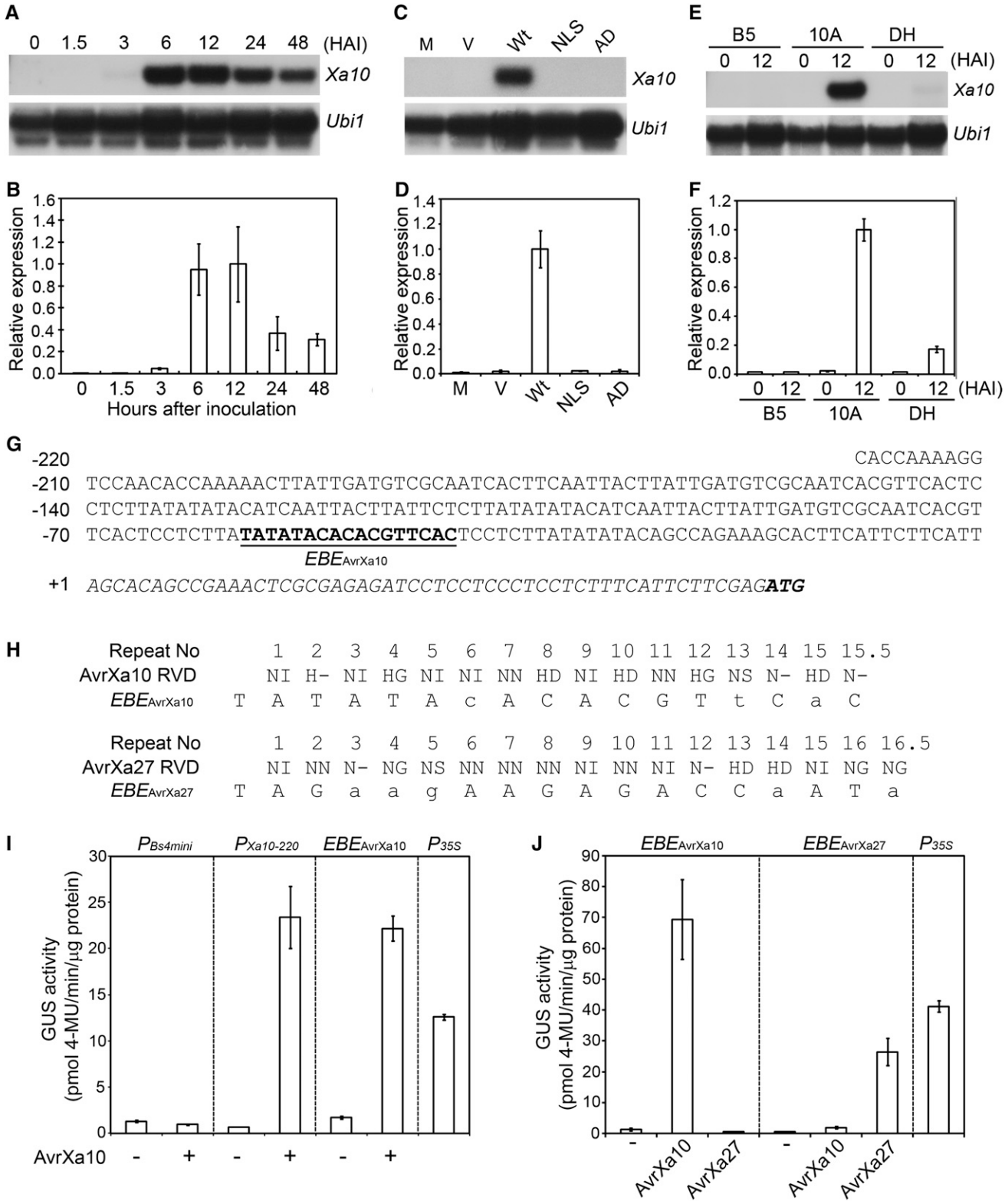

Figure 2. Specific Induction of *Xa10* by AvrXa10.

(A) and **(B)** The expression of *Xa10* in IRBB10A at different time points after inoculation with *X. oryzae* pv *oryzae* strain PXO99^{A}(*avrXa10*). *Xa10* transcripts were detected by RNA gel blot analysis **(A)** and qRT-PCR **(B)**. The expression of rice ubiquitin gene 1 (*Ubi1*) served as control. For qRT-PCR,

that 6xHis-AvrXa10 and 6xHis-AvrXa27 fusion proteins specifically bound the $EBE_{AvrXa10}$ probe and $EBE_{AvrXa27}$ probe, respectively (Supplemental Figures 7A to 7C). The specific probe bindings were outcompeted by the respective nonlabeled $EBE_{AvrXa10}$ and $EBE_{AvrXa27}$ probes, but not by nonspecific probes (Supplemental Figure 7D). Specific interactions between AvrXa10 and $EBE_{AvrXa10}$ and between AvrXa27 and $EBE_{AvrXa27}$ were also observed in yeast using a one-hybrid assay (Supplemental Figures 8A to 8C).

XA10 Triggers an HR in Rice and *N. benthamiana*

Initial attempts failed to generate transgenic rice containing *Xa10* under the control of the cauliflower mosaic virus 35S promoter, possibly due to the lethal effect of *Xa10* at high expression levels. Rice plants with low expression levels of *Xa10*, designated as $Xa10^{w}$, were therefore generated by pyramiding the native *Xa10*, *xa5*, and a plant-expressed version of *avrXa10* under the control of the rice *PR1* gene promoter (genotype: *Xa10xa10*, *xa5xa5*, P_{PR1}*:avrXa10:*T_{Nos}). $Xa10^{w}$ displayed constitutive but weak expression of *avrXa10* and *Xa10* (Supplemental Figures 9A and 9B). The $Xa10^{w}$ plants exhibited resistance to $PXO99^{A}$(*avrXa10*) and reduced susceptibility to $PXO99^{A}$ (Supplemental Figure 9C). Compared with normal rice plants, the $Xa10^{w}$ plants developed spontaneous lesions on uninoculated leaves (Figure 3A). Trypan blue staining, which stains dead cells (Bowling et al., 1997), revealed that the cells in the lesion area had undergone cell death (Figure 3B).

The rice *PR1* gene promoter-driven *Xa10* gene (P_{PR1}*:Xa10:*T_{Nos}) was transiently expressed in *N. benthamiana* leaf cells through *Agrobacterium tumefaciens*–mediated infiltration. An HR was induced on *N. benthamiana* leaves 24 to 27 h after infiltration (HAI) with P_{PR1}*:Xa10:*T_{Nos} (Figures 3F to 3H; Supplemental Figures 10A to 10C). In control experiments, no HR or cell death was induced on *N. benthamiana* leaves infiltrated with the rice *PR1* promoter-driven *Xa27* gene (P_{PR1}*:Xa27:*T_{Nos}) or the empty vector pC1300 (Figures 3F to 3H; Supplemental Figures 10A to 10C). Transient expression assays also demonstrated that a set of *Xa10* fusion genes, including P_{PR1}*:Xa10-eGFP:*T_{Nos}, P_{35S}*:Xa10-eGFP:*T_{Nos}, P_{35S}*:Xa10-eCFP:*T_{Nos}, P_{35S}*:mCherry-Xa10:*T_{Nos}, P_{35S}*:Xa10-mCherry:*T_{Nos}, P_{35S}*:mRFP-Xa10:*T_{Nos}, P_{35S}*:Xa10-mRFP:*T_{Nos}, P_{35S}*:Xa10-Flag:*T_{Nos}, P_{35S}*:3xFlag-Xa10:*T_{Nos}, and P_{35S}*:Xa10-3xFlag:*T_{Nos}, also induced HR in *N. benthamiana* (Figures 3F to 3H; Supplemental Figure 10).

XA10 variants were generated and tested for the ability to induce cell death in *N. benthamiana* (Figure 1D). XA10L18K, an L18K replacement variant of XA10 predicted to disrupt the first transmembrane helix of XA10, failed to induce cell death in *N. benthamiana* (Figures 3F to 3H). XA10 was also sensitive to alteration at some basic amino acid residues. Variants XA10R41L, XA10R46I, and XA10R59A all failed to trigger cell death in *N. benthamiana* (Figures 3F to 3H; Supplemental Figures 10A to 10C). XA10 has four Cys residues, but only one Cys replacement, XA10C113T, abolished cell death induction in *N. benthamiana* (Figures 3F to 3H; Supplemental Figures 10A to 10C). Mutation of the ED motif to "QNNQQ" (XA10NQ) also abolished HR induction in *N. benthamiana* (Figures 3F to 3H; Supplemental Figures 10A to 10C). The phenotypes of *Xa10* variant genes were also tested in transgenic rice. Transgenic plants carrying *Xa10* variants under the control of rice *PR1* gene promoter were all susceptible to $PXO99^{A}$(*avrXa10*), whereas one resistant and one moderately resistant transgenic plants were obtained with the P_{PR1}*:Xa10:*T_{Nos} gene (Figure 4; Supplemental Table 3).

Staining with 3,3′-diaminobenzidine (DAB), which stains H_2O_2, a membrane-permeable form of ROS (Levine et al., 1994; Thordal-Christensen et al., 1997), indicated the presence of H_2O_2 in leaf tissue of $Xa10^{w}$ plants and *N. benthamiana* leaves infiltrated with P_{PR1}*:Xa10:*T_{Nos} or P_{PR1}*:Xa10-eGFP:*T_{Nos} genes (Figures 3C and 3I). Little staining was observed in DH plants without AvrXa10, transgenic *avrXa10* plants in *xa5* genetic background without *Xa10* ($L61^{xa5}$), and *N. benthamiana* infiltrated with the

Figure 2. (continued).

the average expression level of *Xa10* in IRBB10A at 12 HAI with $PXO99^{A}$(*avrXa10*) was set as "1." The qRT-PCR experiments were performed in triplicate, and the data are presented as means ± SD.

(C) and **(D)** The expression of *Xa10* in IRBB10A at 12 HAI with water (M) or $PXO99^{A}$ strains harboring pHM1 (V), pHM1avrXa10 (Wt), pHM1avrXa10NLS (NLS), or pHM1avrXa10AD (AD). RNA gel blot analysis **(C)** and real-time RT-PCR **(D)** were performed similarly as described above.

(E) and **(F)** The expression of *Xa10* in IRBB5(B5), IRBB10A(10A), and *Xa10* and *xa5* DH plants at 0 and 12 HAI with $PXO99^{A}$(*avrXa10*). RNA gel blot analysis **(E)** and qRT-PCR **(F)** were performed similarly as described above.

(G) Nucleotide sequence of *Xa10* promoter and $EBE_{AvrXa10}$. The transcriptional initiation site is marked as "+1." Only a short functional region of *Xa10* promoter (−220 to −1), the 5′ untranslated region (in italics), and start codon (in bold italics) are listed. $EBE_{AvrXa10}$ is referenced.

(H) Association between the repeat variable diresidues (RVDs) of AvrXa10 and the nucleotides of $EBE_{AvrXa10}$. The association was predicted based on the codes published previously (Boch et al., 2009; Moscou and Bogdanove, 2009). Perfect matches are shown in capital letters, and the second most common matches are displayed in lowercase letters. The "–" indicates that amino acid 13 is missing in this repeat. The association between the RVDs of AvrXa27 and the nucleotides of $EBE_{AvrXa27}$ is also displayed.

(I) Identification of $EBE_{AvrXa10}$ in *Xa10* promoter. GUS reporter constructs containing the *Xa10* promoter (−220 to −1) ($P_{Xa10\text{-}220}$) or $EBE_{AvrXa10}$ were codelivered via *Agrobacterium* into *N. benthamiana* with 35S-driven *avrXa10* and empty T-DNA (-), respectively. The AvrXa10-activated promoter activity was measured as the GUS activity. The GUS reporter constructs containing minimal tomato *Bs4* promoter ($P_{Bs4mini}$) only (Boch et al., 2009) and the cauliflower mosaic virus 35S promoter (P_{35S}) served as controls. 4-MU, 4-methyl-umbelliferone. The experiments were performed in triplicate and the data are presented as means ± SD.

(J) Specific recognition between $EBE_{AvrXa10}$ and AvrXa10 and between $EBE_{AvrXa27}$ and AvrXa27. The AvrXa10- or AvrXa27-activated promoter activity was measured as the GUS activity as described in **(I)**. $EBE_{AvrXa10}$ and $EBE_{AvrXa27}$ are GUS reporter constructs containing $EBE_{AvrXa10}$ and $EBE_{AvrXa27}$, respectively.

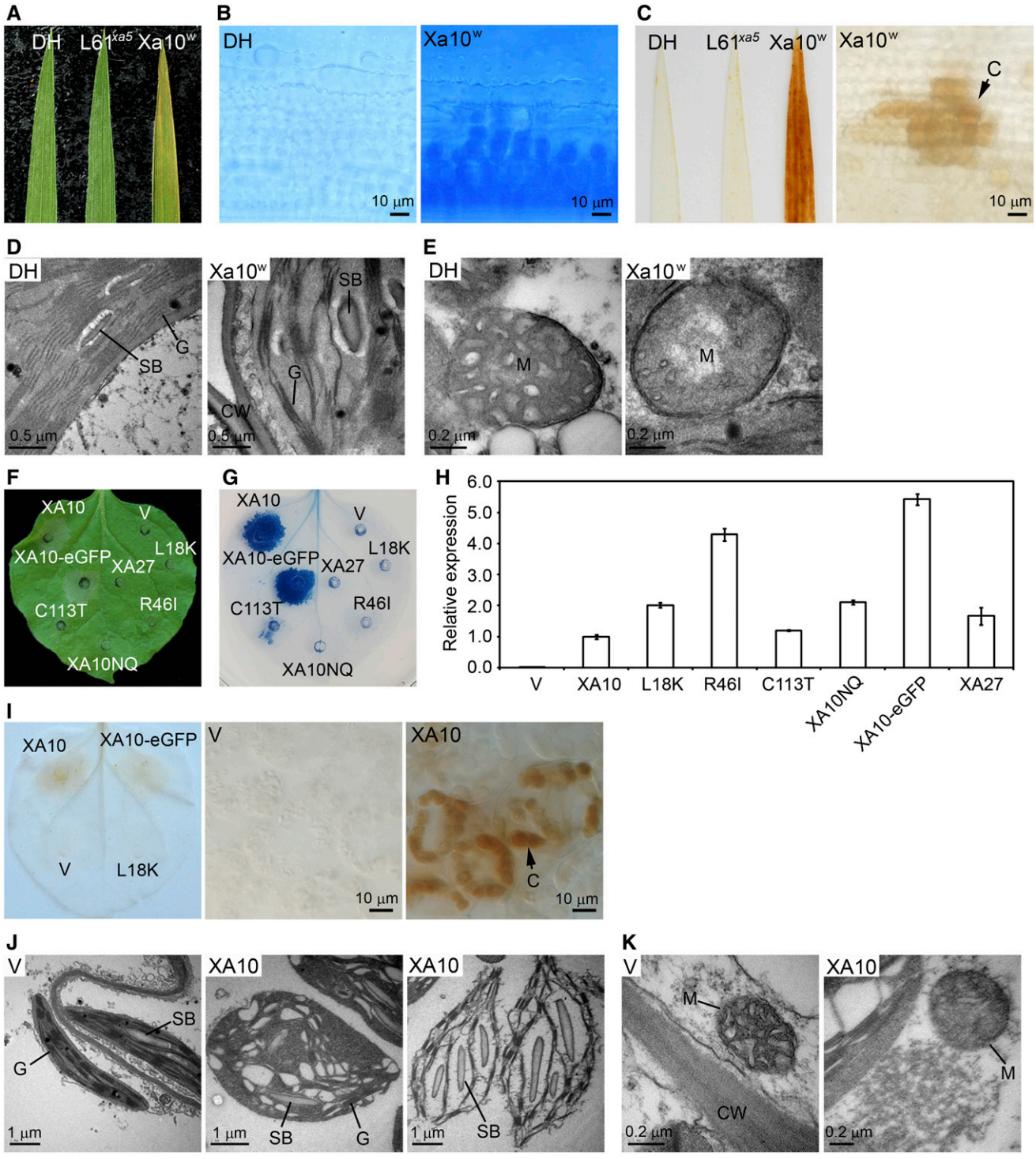

Figure 3. XA10 Induces HR in Rice and *N. benthamiana*.

(A) Phenotypes of rice lines DH(*xa5xa5, Xa10Xa10*), L61^{xa5}(P_{PR1}:*avrXa10*:T_{Nos}, *xa5xa5*), and Xa10^{w}(P_{PR1}:*avrXa10*:T_{Nos}, *xa5xa5, Xa10xa10*) plants at 2 weeks after germination.

(B) Trypan blue staining of leaf tissues of DH and Xa10^{w} plants.

(C) DAB staining of leaf tissues of DH, L61^{xa5}, and Xa10^{w} plants. The high magnification of leaf cells of Xa10^{w} is shown in the right panel. C, chloroplast.

(D) and **(E)** Transmission electron microscopy images of chloroplasts **(D)** and mitochondria **(E)** in leaf cells of DH and Xa10^{w} plants.

P_{PR1}:*Xa10L18K*:T_{Nos} gene or empty vector pC1300 (Figures 3C and 3I). In both rice and *N. benthamiana* cells, H_2O_2 was mainly detected in chloroplasts (Figures 3C and 3I). Chloroplast swelling and degradation were observed during later stages of cell death (Figures 3D and 3J; Supplemental Figure 11). Mitochondrial degradation was also detected in the dying plant cells, which was initiated from the inner membrane of mitochondria (Figures 3E and 3K).

XA10 Induces Apoptosis in HeLa Cells

The *Xa10-eGFP* fusion gene was transiently expressed in the human epithelial carcinoma cell line (HeLa) under the control of human cytomegalovirus immediate-early promoter. Cell death was evident as early as 12 h after transfection (HAT), and dying cells were observed up to 48 HAT. The morphology of cell death resembled apoptosis, including cell shrinkage, nuclear contraction, and distortion, followed by extensive blebbing (Figure 5A). Under cell culture conditions, these apoptotic cells eventually entered postapoptotic necrosis or secondary necrosis stage based on Annexin-V-FLUOS (Annexin V) and propidium iodide (PI) staining (Figure 5B). The apoptotic cells were only stained by Annexin V, whereas the necrotic cells were stained by both Annexin V and PI, or only PI. HeLa cells expressing XA10R46I-eGFP showed a similar morphological phenotype to that of the control cells, which expressed eGFP (Figure 5A). A fluorescence-activated cell sorting assay was used to count apoptotic and necrotic cells in HeLa cells expressing eCFP, XA10-eCFP, or eCFP-fused XA10 variants (Figure 5C). At 48 HAT, 21.7% of the XA10-eCFP–expressing cells were apoptotic, whereas 52.7% (40.3% + 12.4%) of the cells were necrotic (Figure 5C). In control experiments, only 2 and 4.4% (2.9% + 1.5%) of the eCFP-expressing cells were apoptotic and necrotic, respectively (Figure 5C). Cell death was significantly reduced in HeLa cells expressing the XA10 variants XA10R46I-eCFP, XA10L18K-eCFP, XA10R41L-eCFP, XA10R59A-eCFP, XA10C113T-eCFP, and XA10NQ-eCFP (Figure 5C; Supplemental Figure 12). In HeLa cells, cytochrome *c* is released to the cytosol by mitochondria upon apoptotic stimulation (Liu et al., 1996). The cytochrome *c* release was detected in XA10-eGFP–expressing cells, but not in the cells expressing XA10R46I-eGFP or control eGFP (Figure 5D). The elevated level of cytochrome *c* in the cytosol of XA10-eGFP–expressing cells was initially detected at 32 HAT (Figure 5D). It remained at the similar low level at 40 HAT and reached a very high level at 48 HAT (Figure 5D). To determine whether the XA10-induced apoptosis is caspase dependent, z-VAD (*N*-benzyloxycarbonyl-Val-Ala-Asp-fluoromethylketone), a general caspase inhibitor, was applied to HeLa cells expressing XA10-eCFP. At 24 HAT, the percentage of apoptotic cells in XA10-eCFP–expressing cells was significantly reduced from 24.0% in the control experiments to 9.1% in the experiments treated with 20 μM z-VAD (Figure 5E). However, z-VAD did not completely prevent XA10-induced cell death as the percentage of necrotic cells increased from 30.4% in the control experiments to 45.2% in the treatment experiments (Figure 5E). The results indicate that z-VAD switched XA10-induced apoptotic cell death to necrotic cell death.

XA10 Is Localized to the Endoplasmic Reticulum Membrane

Secondary protein structure analysis indicated that XA10 might be a transmembrane protein. Indeed, an initial subcellular localization study showed that XA10-eGFP was localized to the nuclear envelope and the peripheral ER in comparison to the control eGFP, which was localized to cytoplasm and nuclei of *N. benthamiana* leaf cells (Supplemental Figure 13). Further experiments demonstrated that XA10-mCherry and the ER membrane marker eGFP-RcDGAT2 colocalized to the ER membrane in *N. benthamiana* leaf cells (Figure 6A). Likewise, XA10-mRFP and the ER membrane marker eGFP-Sec61β colocalized to the ER membrane in HeLa cells (Figure 6B). In addition, the eGFP-tagged nonfunctional XA10 variants also localized to the ER membrane in both *N. benthamiana* (Supplemental Figure 14) and HeLa cells (Supplemental Figure 15).

The topography of XA10 on the ER membrane was characterized by selective immunofluorescence of cytosol-located antigen after treatment with Triton X-100 or digitonin. Low concentrations of digitonin selectively permeabilize plasma membranes and leave the ER membrane intact, whereas Triton X-100 perforates both, thus allowing the selective immunodetection of cytosol-located antigen when using digitonin (Dyer and Mullen, 2001). Both mCherry-XA10 and XA10-mCherry were labeled with anti-mRFP antibody in rice protoplasts treated with either digitonin or Triton X-100 (Figure 6C). The immunofluorescence signal strength of the two fusion proteins was similar to that of the cytosolic mCherry but different from that of the luminal ER protein mCherry-HDEL, which was only labeled with anti-mRFP antibody after the cells were treated with Triton X-100 (Figure 6C). Similar results were obtained in HeLa cells expressing mRFP-XA10, XA10-mRFP, mRFP, or mRFP-KDEL (Supplemental Figure 16). The results

Figure 3. (continued).

(F) Phenotype of *N. benthamiana* leaf at 24 HAI with *A. tumefaciens* harboring *Xa10* or derivatives. V, pC1300; XA10, P_{PR1}:*Xa10*:T_{Nos}; L18K, P_{PR1}:*Xa10L18K*:T_{Nos}; R46I, P_{PR1}:*Xa10R46I*:T_{Nos}; C113T, P_{PR1}:*Xa10C113T*:T_{Nos}; XA10NQ, P_{PR1}:*Xa10NQ*:T_{Nos}; XA10-eGFP, P_{PR1}:*Xa10-eGFP*:T_{Nos}; XA27, P_{PR1}:*Xa27*:T_{Nos}.

(G) Trypan blue staining of leaf tissue of *N. benthamiana* in **(F)**.

(H) Relative expression of transgenes in leaf tissues of *N. benthamiana* at 20 HAI. Gene transcripts were detected by qRT-PCR. The average expression of P_{PR1}:*Xa10*:T_{Nos} (XA10) was set as "1." The qRT-PCR experiments were performed in triplicate, and the data are presented as means ± SD.

(I) DAB staining of *N. benthamiana* leaf at 14 HAI with *A. tumefaciens* harboring *Xa10* or derivatives.

(J) and **(K)** Transmission electron microscopy images of chloroplasts **(J)** and mitochondria **(K)** in leaf cells of *N. benthamiana* at 14 HAI with *A. tumefaciens* harboring *Xa10* construct or pC1300.

CW, cell wall; G, grana; M, mitochondrion; SB, starch body. Gene abbreviations in **(G)** to **(K)** are the same as in **(F)**. Bars are indicated.

Figure 4. Disease Phenotypes and Gene Expression of Transgenic Lines Carrying *Xa10* Variant Genes.

Disease phenotypes of transgenic T1 plants and control varieties were recorded at 14 d after inoculation with PXO99^{A}(*avrXa10*). Relative expression of *Xa10* and variants in rice plants was determined by qRT-PCR using total RNA isolated from leaves infiltrated with PXO99^{A}(*avrXa10*). The expression of rice *Ubi1* gene served as control. The average expression level of *Xa10* in Xa10NB at 24 HAI was set as "1" (indicated with an asterisk). The experiments were performed in triplicate, and the data are presented as means ± SD. Experiments were repeated three times with T0, T1, and T2 plants of transgenic lines with similar results, and only the data from the T1 generation are presented. NB, Nipponbare; L162, T1 plant of line 162 of P_{PR1}:*Xa10*:T_{Nos}; Xa10NB, *Xa10* in Nipponbare genetic background; L18K L17, T1 plant of line 17 of P_{PR1}:*Xa10L18K*:T_{Nos}; R41L L8, T1 plant of line 8 of P_{PR1}:*Xa10R41L*:T_{Nos}; R46I L18, T1 plant of line 18 of P_{PR1}:*Xa10R46I*:T_{Nos}; R59A L33, T1 plant of line 33 of P_{PR1}:*Xa10R59A*:T_{Nos}; C113T L14, T1 plant of line 14 of P_{PR1}:*Xa10C113T*:T_{Nos}; Xa10NQ L33, T1 plant of line 33 of P_{PR1}:*Xa10NQ*:T_{Nos}.

indicate that both the N and C termini of XA10 are localized to the cytosolic side of the ER (Supplemental Figure 2C). The results also indicate that XA10 might have an internal signal-anchor sequence because both N-terminal and C-terminal XA10 fusion proteins localized to the ER membrane and remained functional.

XA10 Forms Hexamers on the ER Membrane

A fluorescence resonance energy transfer (FRET)–based assay was used to assess for possible intermolecular interactions between XA10 monomers. *N. benthamiana* cells coexpressing XA10-eGFP and XA10-mCherry exhibited a significant FRET signal between the two proteins (Figure 7A). A similar FRET signal was also detected in HeLa cells coexpressing XA10-eGFP and XA10-mRFP (Supplemental Figure 17A). In both experiments, no FRET was detected between eGFP and XA10-mCherry in *N. benthamiana* cells or between eGFP and XA10-mRFP in HeLa cells (Figure 7A; Supplemental Figure 17A). Acceptor photobleaching was used to verify the FRET between XA10-eGFP and XA10-mRFP in HeLa cells. The destruction of XA10-mRFP (acceptor) resulted in the loss of quenching of the XA10-eGFP (donor) fluorescence (Supplemental Figures 17B and 17C). Physical interaction between XA10 proteins was also detected by coimmunoprecipitation (Co-IP) of XA10-mCherry and XA10-3xFlag, which were expressed transiently in rice protoplasts (Figure 7B), and of 3xFlag-XA10 and mRFP-XA10 expressed transiently in HeLa cells (Supplemental Figure 17D). The results from the FRET and Co-IP assays indicate that XA10 forms homooligomers on the ER membrane. Blue Native (BN)–PAGE and immunoblot analysis were then used to determine the molecular weight of XA10 homooligomers from both rice protoplasts expressing XA10-3xFlag (Figures 7C and 7D) and HeLa cells expressing 3xFlag-XA10 (Supplemental Figures 17E and 17F). A major band and a faint band of XA10-3xFlag were detected in the gel (Figure 7C). The major band had an average molecular size of 104.5 ± 4.2 kD, which gives a 6.2 size ratio of the oligomer to the monomer of the fusion protein (molecular mass = 16.9 kD) (Figure 7D). The result indicates that XA10-3xFlag mainly occurs as hexamers in the ER of rice cells. Hexamers were also detected as the major oligomer of 3xFlag-XA10 in HeLa cells (Supplemental Figure 17E). The average molecular size of the most abundant 3xFlag-XA10 oligomer in HeLa cells was 101.8 ± 3.9 kD, giving about a 6.1 size ratio of the oligomer to the monomer of the protein (molecular mass = 16.7 kD) (Supplemental Figure 17F). Oligomers larger than the hexamers were also detected in HeLa cells expressing 3xFlag-XA10 (Supplemental Figure 17E). The monomers of XA10-3xFlag and 3xFlag-XA10 were readily detected by Co-IP analysis (Figure 7B; Supplemental Figure 17D). However, monomers of either fusion protein were not detected by BN-PAGE and immunoblot analysis (Figure 7C; Supplemental Figure 17E). Oligomers and monomers of the 3xFlag-tagged nonfunctional XA10 variants were also detected in rice protoplasts by BN-PAGE- and SDS-PAGE-based immunoblot analyses (Supplemental Figures 18A and 18B).

XA10 Induces ER Ca^{2+} Depletion

The predicted transmembrane helices of XA10 show low similarity to those of Orai proteins, which form hexameric calcium release–activated calcium channels on plasma membranes (Feske et al., 2006; Prakriya et al., 2006; Hou et al., 2012) (Supplemental Figure 19). XA10 also exhibits low similarity to a Na^{+}/Ca^{2+} antiporter (YP_002941808) from the bacterium *Kosmotoga olearid* TBF 19.5.1 (identities = 19/67 [28%], positives = 38/67 [57%], E value = 5.8) and a CaCA Ca^{2+} antiporter (ZP_08938941) from the bacterium *Neisseria wadsworthii* 9715 (identities = 22/80 [28%], positives = 39/80 [49%], E value = 7.9) (Supplemental Figure 20). Protein structure prediction through

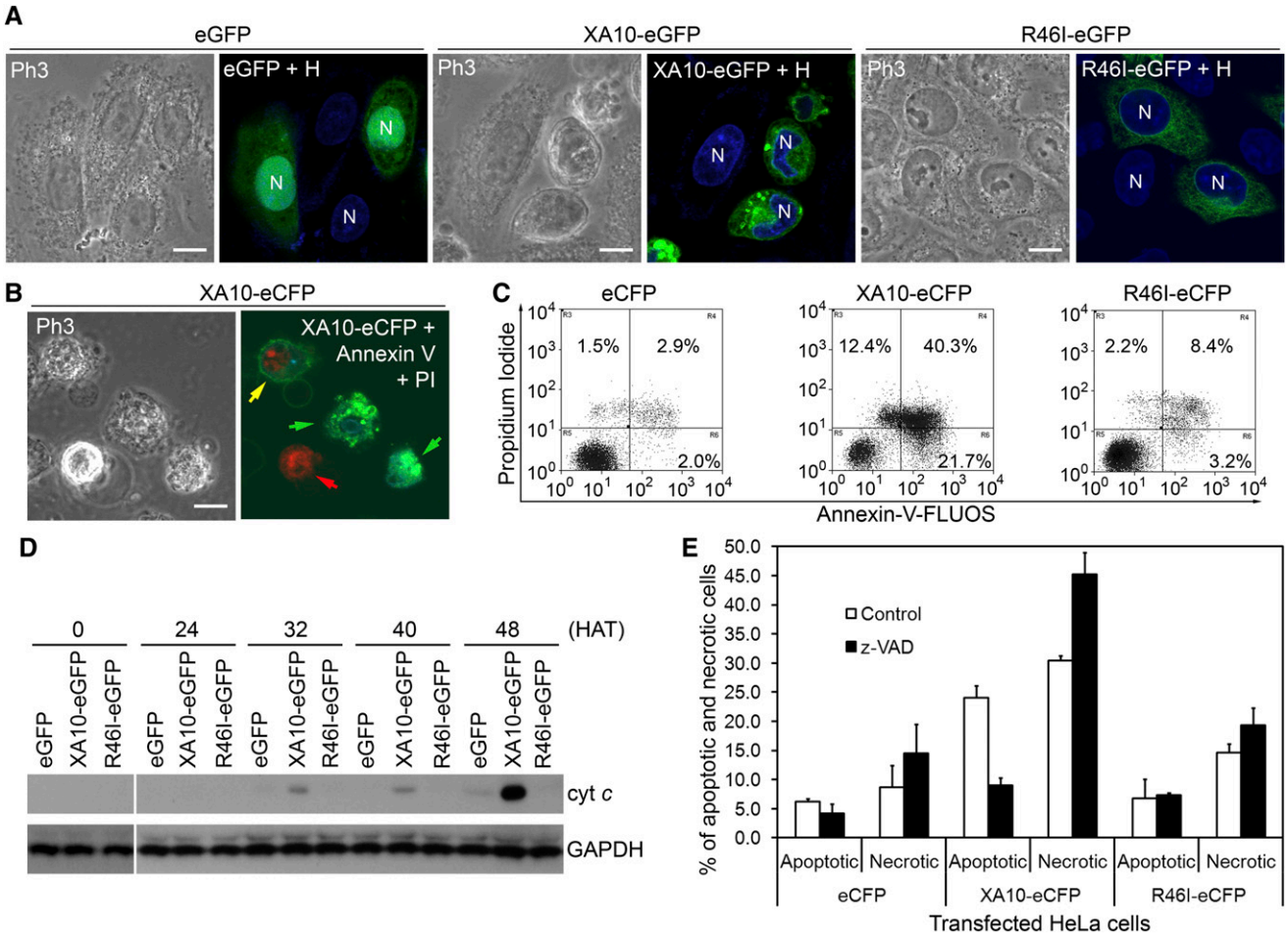

Figure 5. XA10 Induces Cell Death in HeLa Cells.

(A) Phenotypes of HeLa cells expressing eGFP, XA10-eGFP, or XA10R46I-eGFP (R46I-eGFP). Images were taken at 24 HAT. The nuclei of HeLa cells were stained with Hoechst 33258 (H). The bright-field images (Ph3) were taken simultaneously using Phase Contrast 3 optics. N, nucleus. Bars = 10 μm.
(B) Double staining of HeLa cells expressing XA10-eCFP with Annexin V and PI. The apoptotic cells (indicated with green arrows) were stained with Annexin V (green channel), whereas the necrotic cells derived from postapoptotic cell death were stained with both Annexin V and PI (red channel) (indicated with yellow arrow) or PI alone (indicated with red arrow). Images were taken at 24 HAT. Bar = 10 μm.
(C) Flow cytometry analysis of HeLa cells expressing eCFP, XA10-eCFP, or XA10R46I-eCFP (R46I-eCFP) at 48 HAT.
(D) Measurement of cytochrome *c* in cytosol of HeLa cells at different time points after transfection. Cytosolic proteins were separated by SDS-PAGE. Cytochrome *c* (cyt *c*) was detected by anti-cytochrome *c* antibody. GAPDH was detected by anti-GAPDH antibody and served as protein loading control.
(E) Percentage of apoptotic and necrotic cells counted by flow cytometry analysis at 24 HAT in the presence of 20 μM z-VAD.
The experiments were repeated three times with similar results, and the representative images or results are presented.

Phyre2 (http://www.sbg.bio.ic.ac.uk/phyre2/html/page.cgi?id=index) also indicates that the domain at residues 58 to 99 in XA10 as a structure similar to the membrane translocation domain of colicin, a pore-forming bacterial toxin (aligned, 42; modeled, 42; confidence, 26.1%; identity, 24%) (Parker et al., 1989). The potential of XA10 to form ion channels or protein pores on the ER membrane and disturb the calcium homeostasis in the ER was assessed. The concentration of free Ca^{2+} in the ER lumen, cytosol, or mitochondria of *N. benthamiana* or HeLa cells expressing XA10 or variants was measured. The ER Ca^{2+} concentration in the XA10-mCherry–expressing *N. benthamiana* cells, as measured by the Ca^{2+} indicator YC4.60ER, was ~27.6 and 20.7% lower than that in the control cells that expressed mCherry and XA10R46I-mCherry, respectively (Figures 8A and 8B). At the same time, the cytosolic Ca^{2+} concentration in the XA10-mCherry–expressing *N. benthamiana* cells, measured by the Ca^{2+} indicator YC3.60, was 47.3 and 57.8% higher than that in the control mCherry-expressing cells and XA10R46I-mCherry–expressing cells, respectively (Figures 8C and 8D). The results demonstrate that Ca^{2+} depletion in the ER is associated with the presence of XA10 and is accompanied by a cytosolic Ca^{2+} increase. ER Ca^{2+} depletion, as measured by the Ca^{2+} indicator D1ER, was also detected in HeLa cells expressing XA10-mRFP. The ER Ca^{2+} concentration was 33.3% lower than that in mRFP-expressing

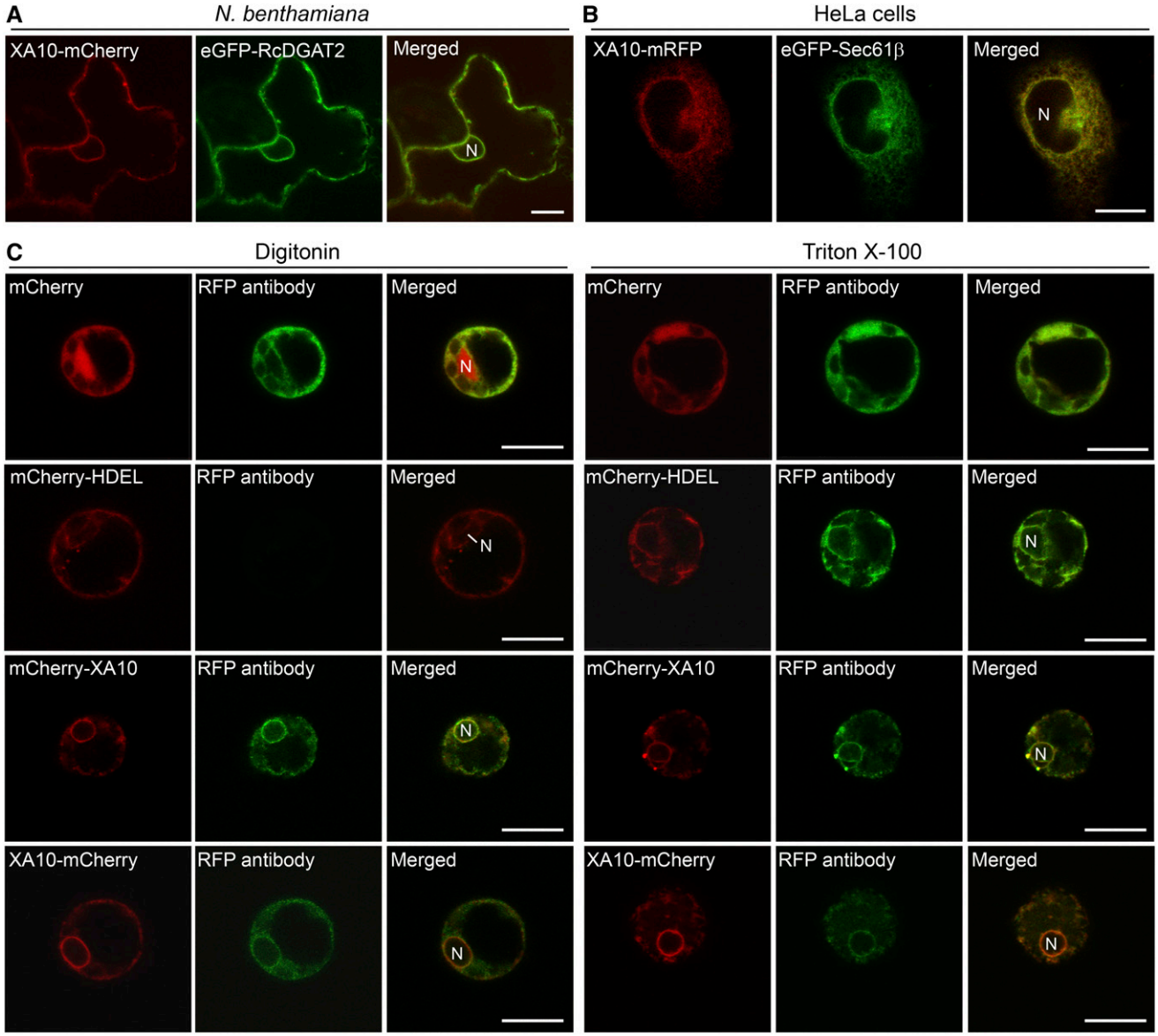

Figure 6. XA10 Is Localized to the ER Membrane.

(A) Subcellular localization of XA10-mCherry and eGFP-RcDGAT2 in leaf cells of *N. benthamiana*. Images were taken at 24 HAI. N, nucleus. Bar = 10 μm.
(B) Subcellular localization of XA10-mRFP and eGFP-Sec61β in HeLa cells. Images were taken at 18 HAT. Bar = 10 μm.
(C) Topography study of XA10 on the ER membrane in rice protoplasts. Protoplasts of rice leaf sheath cells expressing mCherry, mCherry-HDEL, mCherry-XA10, and XA10-mCherry were fixed at 5 HAT and permeabilized using either digitonin (left panel) or Triton X-100 (right panel) before immunofluorescence labeling with anti-RFP monoclonal antibody. Bars = 10 μm.
The experiments were repeated at least three times with similar results, and the representative results are shown here.

HeLa cells and 33.9% lower than that in the XA10R46I-mRFP–expressing cells, respectively (Figures 8E and 8F). However, unlike the cytosolic Ca^{2+} increase in *N. benthamiana* cells, a mitochondrial Ca^{2+} increase was detected in XA10-mRFP–expressing HeLa cells, where the Ca^{2+} concentration, as measured by the Ca^{2+} indicator 4mtD3cpv, was 35.3 and 28.3% higher than that in the mRFP-expressing HeLa cells and XA10R46I-mRFP–expressing cells, respectively (Figures 8G and 8H). The ER Ca^{2+} depletion occurred within 1 h in XA10-mCherry–expressing *N. benthamiana* leaf cells (Figure 8I; Supplemental Figure 21 and Supplemental Movies 1 to 3) and 2 to 3 h in XA10-mRFP–expressing HeLa cells, respectively, after the onset of the process (Figure 8J). The morphology of cells and the ER remained normal during the later stages of ER Ca^{2+} depletion in both *N. benthamiana* and HeLa cells, indicating that this XA10-induced ER Ca^{2+} depletion precedes cell death induction in both kinds of cells (Figures 8A, 8C, 8E, and 8G).

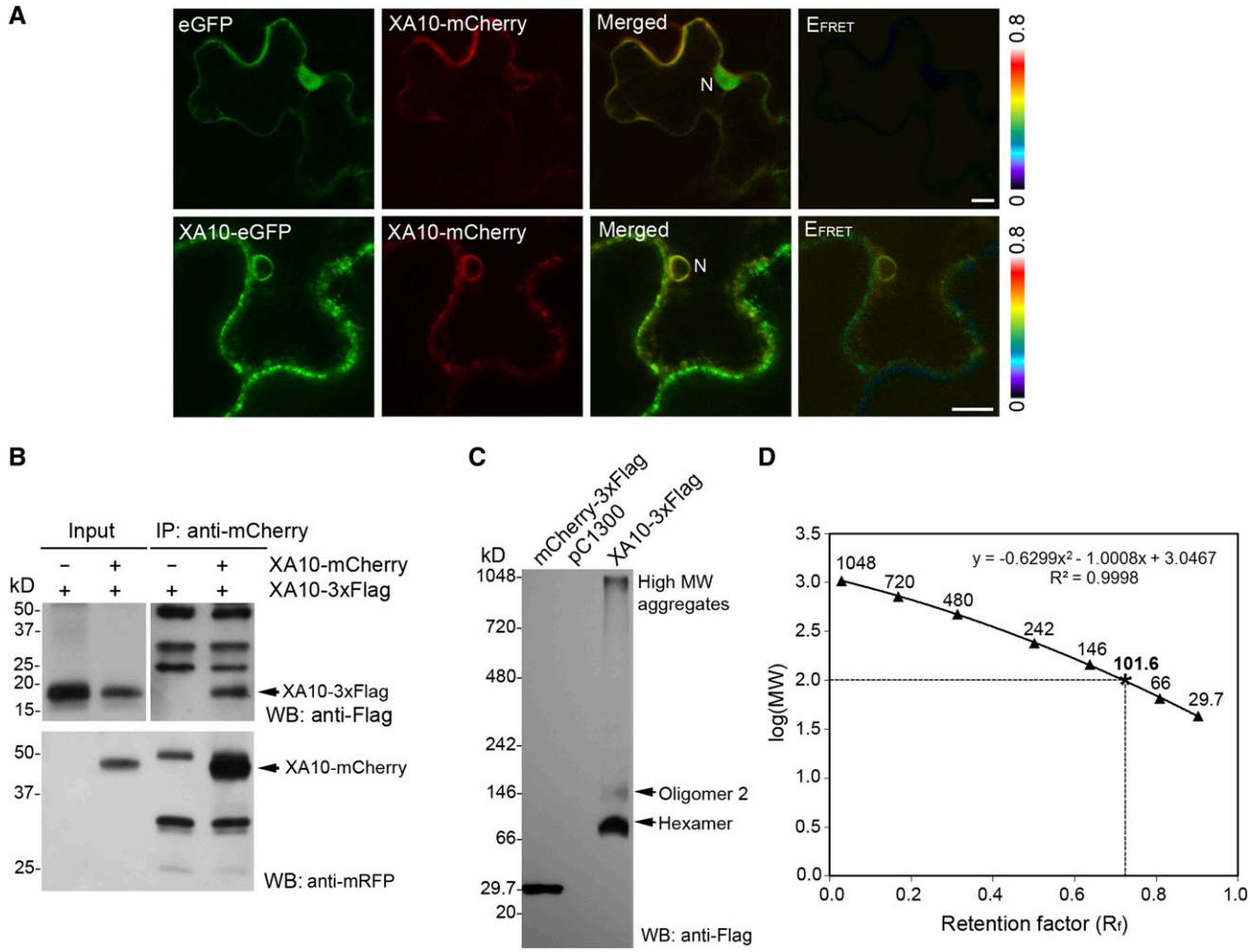

Figure 7. XA10 Forms Oligomers on the ER Membrane.

(A) FRET analysis for interaction between XA10-eGFP and XA10-mCherry coexpressed in *N. benthamiana* leaf cells. Pseudocolored bar of FRET is indicated. N, nucleus. Bars = 10 μm.

(B) Co-IP analysis for protein interaction between XA10-mCherry and XA10-3xFlag coexpressed in rice protoplasts. XA10-mCherry was detected with anti-mRFP antibody while XA10-3xFlag was probed with anti-Flag antibody.

(C) Detection of XA10-3xFlag oligomers using BN-PAGE. 3xFlag-tagged proteins were detected with anti-Flag antibody. XA10-3xFlag oligomers are indicated with arrows. MW, molecular mass; pC1300, control empty vector.

(D) Measurement of molecular size of XA10-3xFlag oligomers. The second-order polynomial best fit was used to plot the retention factor (R_f) values versus log molecular mass. The asterisk denotes the position of XA10-3xFlag hexamer on the curve. Experiments were repeated at least three times. The data shown here are the representative results of one typical experiment.

DISCUSSION

The results presented here indicate that *Xa10* belongs in the class of *R* genes that we refer to here as the TAL effector–inducible terminator *R* gene class, which includes *Xa27* in rice and *Bs3* and *Bs4C-R* in pepper; these *R* genes are characterized by TAL effector–dependent expression (Gu et al., 2005; Römer et al., 2007; Strauss et al., 2012). Multiple lines of evidence presented here corroborate that *Xa10* is indeed the target of AvrXa10. The gene is expressed in an AvrXa10-dependent manner, and transfer of the *Xa10* ORF and immediately adjacent sequences into susceptible cultivars also confers AvrXa10-dependent specific resistance. A functional $EBE_{AvrXa10}$ is found in the promoter region and directs AvrXa10-dependent expression in *N. benthamiana*. Finally, we show that AvrXa10 binds preferentially to an oligonucleotide containing the predicted $EBE_{AvrXa10}$. Furthermore, constitutive and weak expression of the *Xa10* in rice induces a lesion mimic-like phenotype.

Membership in the terminator *R* gene class, at present, is based solely on the TAL effector–dependent induction of the *R* gene; the biochemical mode of action and evolutionary origins of the terminators themselves are unclear. None of the gene products share identifiable sequence relatedness to other members (Gu et al., 2005; Römer et al., 2007; Strauss et al., 2012). Regardless, all

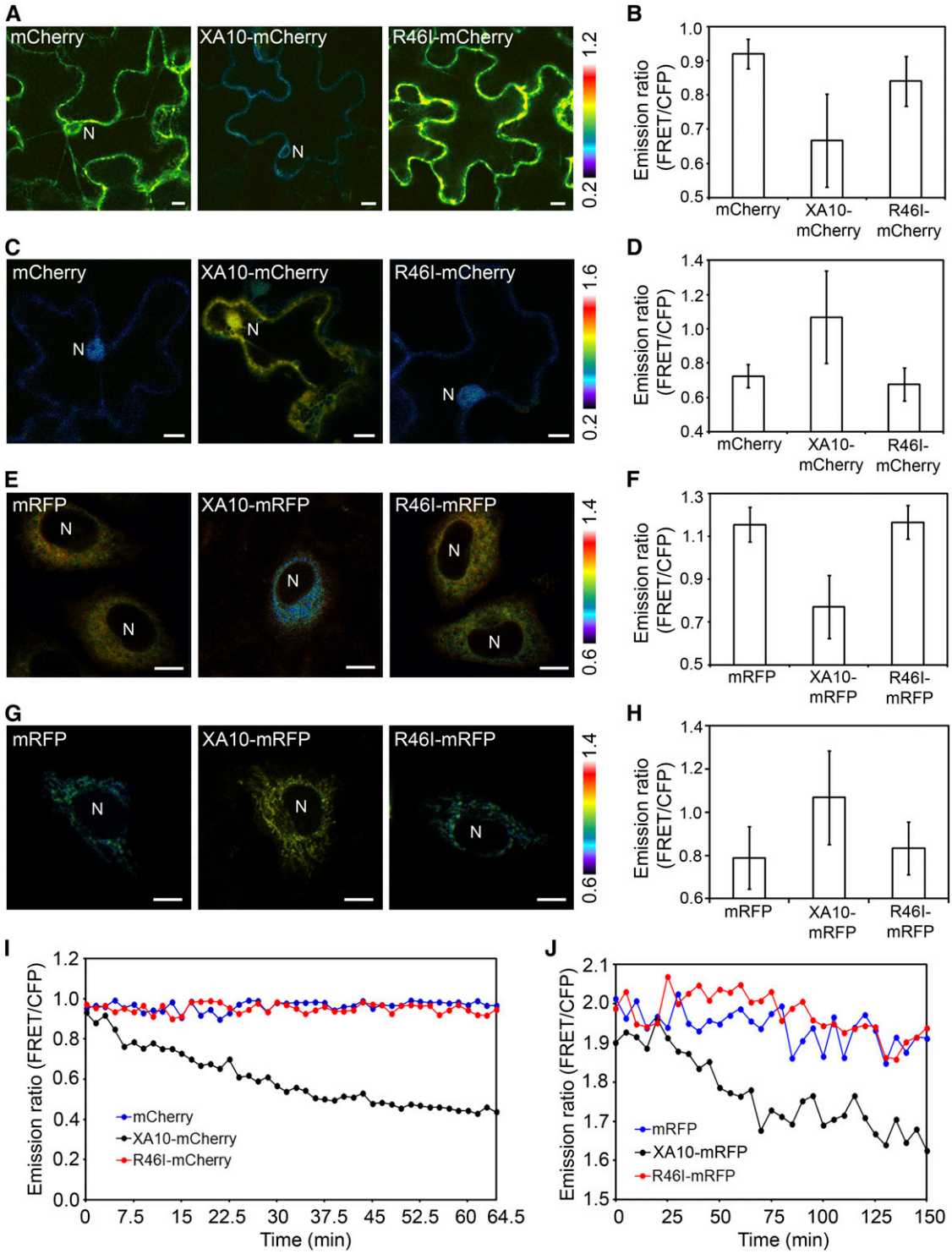

Figure 8. XA10 Induces Calcium Depletion from the ER.

(A) and **(B)** Pseudocolor ratio (FRET/CFP) images **(A)** and average emission ratios (FRET/CFP) **(B)** of YC4.60ER in the ER of *N. benthamiana* leaf cells coexpressing YC4.60ER with mCherry, XA10-mCherry, or R46I-mCherry (XA10R46I-mCherry). Original images were taken at 24 HAI. Cell numbers measured in **(B)**: mCherry, $n = 39$; XA10-mCherry, $n = 32$; R46I-mCherry, $n = 45$. N, nucleus. Bars = 10 μm.

(C) and **(D)** Pseudocolor ratio (FRET/CFP) images **(C)** and average emission ratios (FRET/CFP) **(D)** of YC3.60 in cytosol of *N. benthamiana* leaf cells coexpressing YC3.60 with mCherry, XA10-mCherry, or XA10R46I-mCherry (R46I-mCherry). Original images were taken at 24 HAI. Cell numbers measured in **(D)**: mCherry, $n = 36$; XA10-mCherry, $n = 50$; R46I-mCherry, $n = 42$. Bars = 10 μm.

of the genes function to connect transcriptional activity due to pathogen challenge as mediated by TAL effectors with innate immunity. *Xa10* and *Xa27* have related sequences, limited to rice and closely related wild species, and no clear sequence relatedness to genes of known function. The *Xa27*-resistant and susceptible alleles differ only in the promoter regions and the functional AvrXa27 binding element ($UPT_{AvrXa27}$ box or $EBE_{AvrXa27}$) is only present in the *Xa27* promoter (Gu et al., 2005; Römer et al., 2009). The susceptible cultivars do not have a gene identical to *Xa10*. Nonetheless, the question remains whether *Xa10*, *Xa27*, and related genes have functions in the absence of bacterial challenge. The lack of relatedness in the case of *Xa10* and *Xa27* indicates de novo recruitment of proteins to host defense against *X. oryzae* pv *oryzae*. Structural studies, such as the membrane targeting as discussed in more detail below, may reveal related structural and signaling features that tie the responses to more conserved elements of PCD in plants and animals.

The results here indicate that XA10 functions directly in triggering PCD and that the mode of action is broadly conserved in other plant species and animal cells. A number of XA10 variants localized to the ER and formed hexamers and higher oligomer aggregates, as the wild-type XA10, while failing to induce PCD. The localization of nonfunctional XA10 variants indicates that the effect of XA10 is not simply due to the presence of the heterologous proteins in the ER. The plant HR has been considered to be analogous to apoptosis in animals. However, many of the PCD regulators identified in animals are absent from plant genomes except for a plant ortholog of the *Bax Inhibitor1* (*BI-1*) gene, indicating that plants may use other regulators to control PCD (Arabidopsis Genome Initiative, 2000). Nevertheless, several reports suggest that the plant HR and the animal apoptosis share some properties. For instance, the proapoptotic Bax protein, a member of Bcl-2 protein family in metazoans, functions heterologously in inducing cell death in plant cells, and the *Arabidopsis BI-1* suppresses this cell death (Lacomme and Santa Cruz, 1999; Kawai-Yamada et al., 2001). Inhibitors known to block the activity of caspases in animals are effective at limiting HR in plants (del Pozo and Lam, 1998). Plants were also found to possess HR-dependent caspase-like protease activities and metacaspases (Rojo et al., 2004; Coll et al., 2010). In addition, the plant *BECLIN1* gene negatively regulates PCD through an evolutionarily conserved autophagy pathway (Liu et al., 2005).

Our results also provide insight into the possible biochemical function of XA10. XA10 localizes to the ER membrane of plant and HeLa cells, which is coincidental with the ER Ca^{2+} depletion and the onset of XA10-induced cell death. The ER is an essential organelle of eukaryotic cells, involved in multiple cellular processes that include calcium homeostasis, protein secretion, and lipid biosynthesis. Disturbances in the ER may lead to the cell stress response known as the unfolded protein response, an evolutionarily conserved stress response that can trigger apoptosis if ER dysfunction is severe or prolonged (Shore et al., 2011). The ER is one of the important intracellular Ca^{2+} stores in eukaryotic cells. In the ER, Ca^{2+} supports early protein processing and protein glycosylation. Ca^{2+} may also be involved in subunit assembly and protein folding. Therefore, the reduction of ER Ca^{2+} levels can induce the unfolded protein response (Görlach et al., 2006). The ER is also a key organelle that initiates and modulates apoptosis. ER Ca^{2+} release is an early signaling event for the initiation of apoptosis induced by many apoptotic signals (Pinton et al., 2008). A few prosurvival and proapoptotic proteins of Bcl-2 family are targeted to the ER and control apoptosis through ER calcium homeostasis. For instance, Bax and Bak promote apoptosis by elevating ER Ca^{2+} concentration, triggering ER Ca^{2+} release and its uptake by the mitochondria following stress (Scorrano et al., 2003). It should be noted that the XA10-induced ER Ca^{2+} depletion does not completely resemble Bax/Bak-mediated ER Ca^{2+} release, which increases overall ER Ca^{2+} load and enhances proapoptotic Ca^{2+} release (Scorrano et al., 2003). In XA10-expressing *N. benthamiana* or HeLa cells, no Ca^{2+} increase was observed in the ER before Ca^{2+} release. Nonetheless, the outcome would be expected to be the same regardless of the causes for the change in ER Ca^{2+}. The elevation of cytosolic Ca^{2+} is a critical early step in a signaling cascade involving in plant immune responses. Previous studies demonstrate that the conductance from extracellular and intracellular Ca^{2+} pools contributes to pathogen-associated cytosolic Ca^{2+} elevation (Lecourieux et al., 2006; Ma and Berkowitz, 2007), possibly through ion channels on plasma membrane (Leng et al., 1999; Ma et al., 2006; Qi et al., 2006; Ali et al., 2007) and tonoplast (Kadota et al., 2004; Kurusu et al., 2004; Peiter et al., 2005).

The early signaling in XA10-induced Ca^{2+}-mediated PCD is conserved across plant and animal kingdoms; however, the downstream cell death pathways in the two systems should be

Figure 8. (continued).

(E) and **(F)** Pseudocolor ratio (FRET/CFP) images **(E)** and average emission ratios (FRET/CFP) **(F)** of D1ER in the ER of HeLa cells coexpressing D1ER with mRFP, XA10-mRFP, or R46I-mRFP (XA10R46I-mRFP). Original images were taken at 14 HAT. Cell numbers measured in **(F)**: mRFP, $n = 64$; XA10-mRFP, $n = 65$; R46I-mRFP, $n = 85$. Bars = 10 μm.

(G) and **(H)** Pseudocolor ratio (FRET/CFP) images **(G)** and average emission ratios (FRET/CFP) **(H)** of 4mtD3cpv in mitochondria of HeLa cells coexpressing 4mtD3cpv with mRFP, XA10-mRFP, or R46I-mRFP. Calcium concentration was measured with Ca^{2+} indicator 4mtD3cpv. Original images were taken at 14 HAT. Cell numbers measured in **(H)**: mRFP, $n = 55$; XA10-mRFP, $n = 66$; R46I-mRFP, $n = 59$. Bars = 10 μm.

(I) Change of average emission ratios (FRET/CFP) of YC4.60ER in the ER of *N. benthamiana* cells coexpressing YC4.60ER with mCherry, XA10-mCherry, or XA10R46I-mCherry for over 64.5 min. Original images were traced at ~24 to 27 HAI.

(J) Change of average emission ratios (FRET/CFP) of D1ER in the ER of HeLa cells coexpressing D1ER with mRFP, XA10-mRFP, or XA10R46I-mRFP for over 150 min. Original images were traced at ~14 to 18 HAT.

The experiments were repeated at least three times, and the representative results are presented here. Pseudocolor scale bars indicate the FRET: CFP ratio.

different. While the function of mitochondria in XA10-induced PCD in plant cells remains to be determined, the XA10-induced ROS generation in chloroplasts was detected in rice and *N. benthamiana* cells. Chloroplast-generated ROS has been found to be involved in HR-like cell death mediated by a mitogen-activated protein kinase cascade (Liu et al., 2007) and plays a major role in localized cell death during the non-host interaction between tobacco and *X. campestris* pv *vesicatoria* (Zurbriggen et al., 2009). XA10 may activate a conserved cell death pathway in plants starting with the ER Ca^{2+} depletion that in turn leads to ROS generation in chloroplasts and, ultimately, cell death. In this scenario, it is interesting to know how the Ca^{2+} elevation in the cytosol of plant cells will activate downstream cell death pathways, especially the ROS generation in chloroplasts. In HeLa cells, mitochondria should play an important role in XA10-induced apoptosis. The Ca^{2+} elevation in mitochondria most likely resulted from the rapid Ca^{2+} trafficking through the microdomains between the ER and mitochondria (Rizzuto et al., 1998). The Ca^{2+} overload in mitochondria impairs its respiration and leads to membrane potential drop, mitochondria swelling, and finally the release of apoptotic factors (Luo et al., 2005; Mathai et al., 2005). In this study, the release of cytochrome *c* from mitochondria to cytosol was detected in HeLa cells expressing XA10-eGFP. The release of cytochrome *c* in turn activates caspase, which then cleaves intracellular substrates, resulting in apoptosis (Li et al., 1997). The caspase inhibitor z-VAD does not block XA10-induced cell death; instead, it only switches apoptosis to necrosis, which is consistent with the previous report (He et al., 2009). In other words, once the XA10-triggered Ca^{2+}-mediated cell death signaling is activated, it will ultimately lead to cell death either through apoptosis, necrosis, or both pathways.

The transmembrane helices of XA10 and the formation of hexamers on the ER membrane are reminiscent of the Orai proteins, which form a calcium release–activated calcium channel on plasma membrane (Feske et al., 2006; Prakriya et al., 2006). Recently, Orai from *Drosophila melanogaster* was found to form a hexamer (Hou et al., 2012). The transmembrane helix 1 (M1) of Orai contains charged amino acid residues. Six M1 helices, one from each subunit, make up an inner ring of helices and line the ion pore (Hou et al., 2012). In this study, the M2 in XA10 contains charged amino acid residues, which are essential for XA10 function. In addition, the above-mentioned proapoptotic and antiapoptotic Bcl-2 proteins also possess channel-forming activity on the ER (Antonsson et al., 1997; Schlesinger et al., 1997). The structures of the Bcl-2 proteins show a striking similarity to the overall fold of the pore-forming domains of bacterial toxins (Petros et al., 2004). Although the protein analyses and the results in this study suggest that XA10 might form a Ca^{2+} channel or protein pore on the ER membrane, direct evidence for pore-forming activity of XA10 remains for future research. Alternatively, XA10 might interact with existing ion pumps or channels on the ER to either suppress the ER Ca^{2+} intake or promote ER Ca^{2+} release. For instance, Bcl-2 functionally interacts with inositol 1,4,5-trisphosphate receptors to regulate calcium release from the ER in response to IP_3 (Chen et al., 2004). In either of the two scenarios, XA10 performs its pathological function by disrupting ER and cellular Ca^{2+} homeostasis, inducing cell death. In rice, the cell death leads to HR, which restricts the growth and spread of *X. oryzae* pv *oryzae* from the infection site to other parts of the plant.

Based on the results obtained in this study, we propose that XA10 is an intrinsic inducer of PCD in rice that functions broadly in both plant and animal cells. *Xa10* and related *R* genes may be the proverbial tip of the iceberg and plants may have co-opted the lesion mimic phenomenon as a disease resistance strategy. *Xa10* should prove useful as a probe of cell death pathways in both monocotyledonous and dicotyledonous plants. *Xa10* may also be useful to engineer inducible resistance in both monocotyledonous and dicotyledonous plants (Ayliffe et al., 2002; Römer et al., 2009).

METHODS

Rice Lines and Growth Conditions

IRBB10A is an improved near-isogenic line of *Xa10* in the IR24 genetic background (Gu et al., 2008). Nipponbare is a japonica rice (*Oryza sativa*) cultivar. Xa10NB is another near-isogenic line of *Xa10* in the Nipponbare genetic background. IRBB5 harbors the recessive *xa5* gene in the IR24 background (Iyer and McCouch, 2004). Rice plants were grown in the greenhouse at 32°C for 12.5 h (light) and 25°C for 11.5 h (dark).

Genes and Constructs

The *avrXa10NLS* and *avrXa10AD* mutants were generated previously (Zhu et al., 1998). The *avrXa10* and mutants were cloned into the cosmid vector pHM1 (GenBank accession number EF059993) to generate pHM1avrXa10, pHM1avrXa10NLS, and pHM1avrXa10AD and transferred into *Xanthomonas oryzae* pv *oryzae* strain PXO99^{A}. The luminal ER fluorescent protein markers for plant cells were SP_{Atchit}-mCherry-HDEL (mCherry-HDEL) and SP_{Atchit}-eCFP-HDEL (eCFP-HDEL), in which mCherry or eCFP was fused with an N-terminal signal peptide derived from an *Arabidopsis thaliana* vacuolar basic chitinase and the C-terminal ER retention sequence HDEL (Haseloff et al., 1997). The luminal ER fluorescent protein marker for HeLa cells was $SP_{Calreticulin}$-mRFP-KDEL (mRFP-KDEL), in which mRFP was fused with an N-terminal signal sequence from calreticulin (Palmer et al., 2004) and the C-terminal ER retention sequence KDEL. The ER membrane marker for plant cells was eGFP-RcDGAT2, in which eGFP was fused with type 2 diacylglycerol acyltransferase from caster bean (*Ricinus communis*) (RcDGAT2) (Shockey et al., 2006). The ER membrane marker for HeLa cells was eGFP-Sec61β, in which eGFP was fused with a truncated translocon protein Sec61β of *Neurospora crassa*. The binary constructs containing genes for plant transformation were made with binary vectors pC1300 or pC1305.1 (CAMBIA) and transferred into *Agrobacterium tumefaciens* strains AGL1 or GV3101. The constructs containing genes for HeLa cell transfection were made with vector pcDNA3.1(+) (Invitrogen). GUS reporter constructs were designed based on the GUS reporter vector published previously (Boch et al., 2009) with a slight modification. Ca^{2+} indicator constructs for measurement of Ca^{2+} in the ER and cytosol of plant cells were derived from pSLJAct1-YC4.60ER and pSLJAct1-YC3.60 (Iwano et al., 2009), respectively, by replacing the *Act1* gene promoter with the 35S promoter. Constructs used in this study are listed in Supplemental Table 4.

Rice Transformation

Agrobacterium-mediated transformation of Nipponbare was performed using the method described previously (Hiei et al., 1994).

Bacterial Blight Inoculation

Bacterial inoculation was performed using the leaf-clipping method, and disease scoring was measured as described previously (Gu et al., 2004). Experiments were repeated at least three times or generations.

RNA Gel Blot Analysis

Total RNA was isolated from the leaf tissues using the RNeasy plant mini kits (Qiagen), and poly(A)$^+$ RNA (mRNA) was purified from the total RNA using Oligotex mRNA Midi kits (Qiagen) according to the manufacturer's instructions. About 5 μg mRNA was used for each lane in RNA gel blot analysis. The *Xa10* probe was amplified from *Xa10* coding region using DNA primers SP1F and SP1R (Supplemental Table 5). RNA loading was assessed by hybridizing RNA gel blots to the rice ubiquitin gene 1 (*Ubi1*) probe.

RACE

Xa10 cDNA was isolated using a SMART RACE cDNA amplification kit (Clontech). Both 5′ RACE and 3′ RACE were conducted in accordance with the manufacturer's instructions. The PCR products were cloned into pGEM T-easy vector (Promega) and sequenced. The specific primers for 5′ RACE and 3′ RACE were RGP6-F and GS4R1, respectively (Supplemental Table 5).

Quantitative RT-PCR

Quantitative RT-PCR (qRT-PCR) was performed in accordance with the procedures described previously (Gu et al., 2011). For qRT-PCR in rice, the expression of the rice *Ubi1* gene was used as the internal control. The specific primer pairs for *Xa10* and *Ubi1* were 10RTF2/10RTR2 and RBQ3/RBQ4, respectively (Supplemental Table 5). For qRT-PCR in *Nicotiana benthamiana*, the expression of the glyceraldehyde-3-phosphate dehydrogenase (GAPDH) gene of *N. benthamiana* served as the internal control. The specific primer pair for the fusion genes of *Xa10*, its derivatives, and *Xa27* was TNos-F/TNos-R, which was derived from the *Nos* terminator (Supplemental Table 5). The specific primer pair for the GAPDH gene was NbGAPDH-F/NbGAPDH-R (Supplemental Table 5). The qRT-PCR experiments were performed in triplicate and the data are presented as means ±SD.

Infiltration of *N. benthamiana* with *Agrobacterium*

Suspensions of *Agrobacterium* strain GV3101 harboring binary constructs were infiltrated into leaves of *N. benthamiana* as described previously (Kay et al., 2007). The infiltrated plants were grown under 16 h light and 8 h darkness at 25°C. Phenotype was checked at 24 to 48 HAI. For fluorescence detection, water-mounted sections of leaf tissue were examined using a LSM 510 Exciter Upright confocal microscope system (Carl Zeiss). The excitation/emission combinations for eGFP, eCFP, and mCherry were 488/505- to 530-, 458/475- to 525-, and 543/600- to 650-nm band-passes, respectively. Imaging of FRET between eGFP and mCherry was accomplished using a 488-nm excitation filter and two emission filters, 505- to 530-nm band-pass for eGFP and 600- to 650-nm band pass for FRET channel, alternated by a filter changer.

Detection of ROS

Accumulation of H_2O_2 in plant cells was detected by DAB staining, as described previously (Thordal-Christensen et al., 1997). Briefly, leaf tissues were vacuum-infiltrated in DAB solution (Sigma-Aldrich) for 5 min and incubated at 25°C for 8 h. Samples were then cleared by boiling in 96% ethanol for 5 min. The cleared samples were mounted in 30% lactic acid for microscopy analysis.

Trypan Blue Staining

Cell death in plant tissues was detected by trypan blue staining, as described previously (Bowling et al., 1997). In brief, plant tissues were submerged in a 70°C trypan blue solution (2.5 mg of trypan blue per mL, 25% [w/v] lactic acid, 23% water-saturated phenol, and 25% glycerol) and heated over boiling water for 2 min and left to stain overnight. After destaining in chloral hydrate solution (25 g in 10 mL of water) for 3 d, samples were equilibrated with 70% glycerol for photography or microscopy analysis.

HeLa Cell Culture, Plasmid Transfection, Flow Cytometry, and Confocal Microscopy

HeLa cells were cultured in Dulbecco's minimal essential medium supplemented with 10% fetal bovine serum, 100 units/mL penicillin, and 100 μg/mL streptomycin. Cells grown on glass chamber dishes or 60-mm Petri dishes were transfected with 1 to 2 μg of plasmids using Lipofectamine 2000 (Invitrogen) according to the manufacturer's instruction. At 24 or 48 HAT, cells were rinsed with warm PBS and fixed with 4% paraformaldehyde (EM Sciences) in warm PBS for 10 min. Cells were then rinsed thoroughly three times in PBS. To locate the nucleus, cells were incubated with 1 μg/mL Hoechst 33258 (BD Biosciences) for 10 min at room temperature followed by washing three times with PBS. Flow cytometry of HeLa cells was performed as described previously (Krysko et al., 2008). In brief, the HeLa cells (2×10^5) at 24 or 48 HAT were trypsinized, washed once with binding buffer (10 mM HEPES, pH 7.4, 140 mM NaCl, 1 mM $MgCl_2$, 5 mM KCl, and 2.5 mM $CaCl_2$), and then resuspended in 200 μL binding buffer with 0.5 μg/mL Annexin-V-FLUOS (Annexin V; Roche) and 1 μg/mL PI (BD Biosciences). After incubation for 30 min at room temperature in the dark, the samples were washed once with binding buffer and immediately analyzed on a FACSCalibur flow cytometer (BD Biosciences). For caspase inhibition, the specific caspase inhibitor z-VAD (Singlab) was added to the culture medium at the final concentration of 20 μM. Images of HeLa cells were taken using a LSM 510 Meta confocal microscope system (Carl Zeiss). The excitation/emission combination for eGFP, eCFP, mRFP, Hoechst, Annexin V, and PI were 488/505- to 530-, 458/470- to 500-, 543/560- to 615-, 405/420- to 480-, 488/505- to 530-, and 543/560- to 615-nm band-passes, respectively. Imaging of FRET between eGFP and mRFP was accomplished using a 488-nm excitation filter and two emission filters, 505- to 530-nm band-pass for eGFP and 625- to 690-nm band-pass for FRET channel, alternated by a filter changer. For photobleaching, XA10-mRFP at the selected regions of HeLa cells was photobleached for 400 s. Images were taken before and after photobleaching. The bright-field image was taken simultaneously using Phase Contrast 3 optics.

Transmission Electron Microscopy

Leaf blades of rice at 2 weeks after germination and *N. benthamiana* leaf tissues at 14 HAI were fixed overnight in 2.5% glutaraldehyde in 0.1 M phosphate buffer, pH 7.2. After being briefly rinsed in the buffer, samples were postfixed for 2 h with 1% osmium tetroxide in 0.1 M phosphate buffer, pH 7.2. Samples were dehydrated through a graded series of ethanol before being embedded in Spurr's resin. Ultrathin sections (90 nm) were cut with a diamond knife on an ultramicrotome (Leica Ultracut UCT) and mounted on 300-mesh copper grids. They were then stained with uranyl acetate and lead citrate and examined with a transmission electron microscope (JEM-1230; JEOL) at 120 kV. Photographs were taken with a digital microphotography system (Gatan).

Topography Study of XA10 on the ER Membrane

Topography study of XA10 on the ER membrane in rice cells was conducted using rice protoplasts. Rice protoplast generation and transfection were performed as described previously (Zhang et al., 2011). Rice protoplasts expressing mCherry-XA10, XA10-mCherry, mCherry-HDEL, or mCherry were fixed with 3% paraformaldehyde at 4°C at 5 HAT. The membrane systems of protoplasts were either completely permeabilized with Triton X-100 (0.25% [v/v]) or selectively permeabilized for plasma membrane with digitonin (5 μg/mL). Similarly, HeLa cells transiently expressing mRFP-XA10, XA10-mRFP, mRFP-KDEL, or mRFP were fixed at

18 HAT. The membrane systems of the fixed cells were either completely permeabilized with Triton X-100 (0.2% [v/v]) or selectively permeabilized for plasma membrane with digitonin (7.5 μg/mL). The permeabilized protoplasts and HeLa cells were first stained with anti-mRFP antibody (Abcam; dilution 1:1000) and then with Alexa Fluor 488–conjugated goat anti-mouse antibody (Invitrogen; dilution 1:100). Images of cells were taken using a LSM 510 Meta confocal microscope system (Carl Zeiss).

Co-IP

XA10-mCherry and XA10-3xFlag were coexpressed in rice protoplasts according to the method described previously (Zhang et al., 2011) and solubilized from the ER membrane with RIPA buffer (20 mM Tris-Cl, pH 7.5, 150 mM NaCl, 1 mM EGTA, and 1% Nonidet P-40). Co-IP was performed with the anti-mRFP affinity gel (MBL International) according to the manufacturer's protocol. For Co-IP between 3xFlag-XA10 and mRFP-XA10 in HeLa cells, the immunoprecipitation was performed with the anti-Flag M2 affinity gel (Sigma-Aldrich) according to manufacturer's protocol. The coimmunoprecipitated proteins were analyzed with SDS-PAGE. Immunoblot analysis was performed using anti-mRFP (Abcam) or anti-Flag (Sigma-Aldrich) antibodies, respectively.

BN-PAGE

BN-PAGE was performed as described previously (Wittig et al., 2006). The ER membrane was isolated from rice protoplasts expressing XA10-3xFlag with method described previously (Abas and Luschnig, 2010). The ER membrane proteins were solubilized from the ER membrane with solubilization buffer (50 mM NaCl, 50 mM Bis-Tris-Cl, 2 mM 6-aminocapric acid, 1 mM EDTA, and 4.6% digitonin). The same buffer was also used to solubilize 3xFlag-XA10 proteins from membrane pellets of HeLa cells. Protein samples containing 0.5% Coomassie Blue G 250 were separated in a native 4 to 15% Bis-Tris gradient gel. The protein bands in the gel were electroblotted to a polyvinylidene fluoride membrane for immunoblot analysis using anti-Flag antibody (Sigma-Aldrich). NativeMARK unstained protein standard (Invitrogen) was used as the native molecular mass marker. A second-order polynomial curve fit for plotting the points was used to estimate protein molecular mass.

Measurement of Cytochrome *c* in Cytosol of HeLa Cells

Cytochrome *c* was measured by immunoblotting as described previously with slight modification (Liu et al., 1996). About 20 to 30 mg of HeLa cells were harvested, washed once with ice-cold PBS, and gently lysed in 5 volumes of ice-cold lysis buffer (20 mM HEPES-KOH, pH 7.5, 10 mM KCl, 1.5 mM $MgCl_2$, 1 mM sodium EDTA, 1 mM sodium EGTA, 1 mM DRR, and 0.1 mM phenylmethylsulfonyl fluoride) containing 250 mM Suc. The homogenates were centrifuged twice at 750*g* for 10 min at 4°C to remove nuclei. The supernatants were centrifuged at 13,200*g* at 4°C for 60 min. Proteins from cytosolic fraction were resolved by SDS-PAGE and transferred onto nitrocellulose membranes. Immunoblot analysis was performed using anti-cytochrome *c* antibody (BD Pharminge). GAPDH was detected by anti-GAPDH antibody (Imgenex) and served as protein loading control.

Measurement of Calcium in *N. benthamiana* and HeLa Cells

The free Ca^{2+} in the ER and cytoplasm of *N. benthamiana* cells was detected with Ca^{2+} indicators YC4.60ER and YC3.60, respectively (Iwano et al., 2009). *N. benthamiana* cells at 24 to 36 HAI were imaged for eCFP, eYFP, and FRET using a LSM510 EXCITER upright confocal microscope system (Carl Zeiss). The excitation/emission combinations for mCherry, eCFP, eYFP, and FRET were 543/600- to 650-, 458/475- to 525-, 488/505- to 530-, and 458/505- to 530-nm band-passes, respectively. Time-lapse images of *N. benthamiana* cells at 24 to 36 HAI were captured at 90-s intervals. The free Ca^{2+} in the ER and mitochondria of HeLa cells was measured with Ca^{2+} indicators D1ER and 4mtD3cpv, respectively (Palmer and Tsien, 2006). HeLa cells at 12 to 20 HAT were imaged using an LSM510 Meta confocal microscope system (Carl Zeiss). The excitation/emission combinations for mRFP, eCFP, Citrine, and FRET were 543/560- to 615-, 405/470- to 500-, 488/505- to 550-, and 405/505- to 550-nm band-passes, respectively. Time-lapse images of HeLa cells at 12 to 20 HAT were captured at 5-min intervals using a Nikon Ti-E with perfect focus system (Nikon). The excitation/emission combinations for mRFP, eCFP, Citrine, and FRET were 561/589- to 625-, 405/470- to 490-, 515/525- to 555-, and 405/525- to 555-nm band-passes, respectively.

Images were analyzed using Image J and Metamorph (Universal Imaging). FRET ratios were analyzed using the methods described previously (Palmer and Tsien, 2006). Briefly, after a background subtraction, the FRET ratio was calculated as follows:

$$\text{FRET ratio} = \text{FRET}/\text{CFP} = [I_{DA} - \text{a} \times I_{AA} - \text{c} \times I_{DD}]/[I_{DD} - \text{b} \times I_{AA}]$$

where FRET is correction done FRET; CFP is correction done CFP; I_{DA} is the intensity of uncorrected FRET; I_{AA} is the intensity of eYFP of YC4.60ER (or YC3.60) or Citrine of D1ER (or 4mtD3cpv) only dyed; I_{DD} is the intensity of eCFP of YC4.60ER (or YC3.60) or eCFP of D1ER (or 4mtD3cpv) only dyed; a is the bleed-through coefficient from excited YFP-HDEL or Citrine-KDEL to FRET channel (a = I_{DA}/I_{AA}); b is the bleed-through coefficient from excited YFP-HDEL or Citrine-KDEL to eCFP channel (b = I_{DD}/I_{AA}); and c is the bleed-through coefficient from excited eCFP to FRET channel (c = I_{DA}/I_{DD}).

Accession Number

Sequence data for *Xa10* can be found in the GenBank/EMBL data libraries under accession number JX025645.

Supplemental Data

The following materials are available in the online version of this article.

Supplemental Figure 1. Detection of the *Xa10* Gene in Different Rice Cultivars by DNA Gel Blot Analysis.

Supplemental Figure 2. Transmembrane Helix Prediction of XA10.

Supplemental Figure 3. XA10 and Related Proteins.

Supplemental Figure 4. The Expression of *Xa10* in Transgenic Line L198 after Inoculation with *X. oryzae* pv *oryzae* Strains.

Supplemental Figure 5. The *xa5* Allele Partially Suppresses *Xa10*-Mediated Resistance to Bacterial Blight.

Supplemental Figure 6. GUS Reporter Constructs.

Supplemental Figure 7. AvrXa10 Binds Specifically to *EBE*AvrXa10.

Supplemental Figure 8. The Specific Interaction between *EBE*AvrXa10 and AvrXa10 in Yeast.

Supplemental Figure 9. Generation of *Xa10* Weak Expression Plants (Xa10w).

Supplemental Figure 10. Phenotype of *N. benthamiana* Leaves Transiently Expressing XA10 or Derivatives.

Supplemental Figure 11. Chloroplast Swelling and Cell Death in Leaf Cells of *N. benthamiana* Transiently Expressing XA10.

Supplemental Figure 12. Flow Cytometry Analysis of HeLa Cells Transiently Expressing XA10 or Variants.

Supplemental Figure 13. Subcellular Localization of XA10 in *N. benthamiana* Leaf Cells.

Supplemental Figure 14. Subcellular Localization of XA10 Variants in *N. benthamiana* Leaf Cells.

Supplemental Figure 15. Subcellular Localization of XA10 Variants in HeLa Cells.

Supplemental Figure 16. Topography Study of XA10 on the ER Membrane in HeLa Cells.

Supplemental Figure 17. XA10 Forms Oligomers on the ER Membrane in HeLa Cells.

Supplemental Figure 18. Detection of XA10 Variants Expressed in Rice Protoplasts.

Supplemental Figure 19. Alignment of Amino Acid Sequences of XA10 and Orai Proteins from Human (*Homo sapiens*).

Supplemental Figure 20. XA10 and Bacterial Antiporter Proteins.

Supplemental Figure 21. XA10 Induces ER Calcium Depletion in *N. benthamiana* Cells.

Supplemental Table 1. Number of the Transgenic T0 Plants Obtained from Rice Transformation with Subclones at the *Xa10* Locus.

Supplemental Table 2. Lesion Length and Disease Phenotype of *Xa10* Transgenic Plants at 2 Weeks after Inoculation with PXO99 (*avrXa10*) and PXO99.

Supplemental Table 3. Summary of Transgenic Plants Transformed with *Xa10* or Variants under Rice *PR1* Gene Promoter.

Supplemental Table 4. Constructs Used in This Study.

Supplemental Table 5. DNA Primers Used in This Study.

Supplemental Methods.

Supplemental Movie 1. Time-Lapse Pseudocolor Ratio (FRET/CFP) Images of YC4.60ER in the ER of a *N. benthamiana* Leaf Cell Coexpressing YC4.60ER and mCherry.

Supplemental Movie 2. Time-Lapse Pseudocolor Ratio (FRET/CFP) Images of YC4.60ER in the ER of a *N. benthamiana* Leaf Cell Coexpressing YC4.60ER and XA10-mCherry.

Supplemental Movie 3. Time-Lapse Pseudocolor Ratio (FRET/CFP) Images of YC4.60ER in the ER of a *N. benthamiana* Leaf Cell Coexpressing YC4.60ER and XA10R46I-mCherry.

Supplemental Data Set 1. Text File of Alignment Corresponding to Phylogenetic Analysis in Supplemental Figure 3.

ACKNOWLEDGMENTS

We thank N.R.S. Hamilton and D. Brar for providing rice cultivar IRBB5, J. Boch for *avrXa10* construct, K. Shimamoto for pANDA35HK, R.Y. Tsien for pcDNA3-D1ER and pcDNA3-mt-cameleon, M. Iwano for pSLJAct1-YC4.60ER and pSLJAct1-YC3.60, and G. Jedd for the *Sec61*β gene. The cloning of *Xa10* was supported by the intramural research funds from Temasek Life Sciences Laboratory, a competitive grant from the Agri-Food and Veterinary Authority of Singapore, and a grant from Temasek Foundation. The research on XA10 function was supported by the National Research Foundation Singapore under its Competitive Research Programme (CRP Award NRF-CRP 8-2010-02). F.F.W. received support from the DBI-0820831 from the Plant Genome Research Program of the U.S. National Science Foundation.

AUTHOR CONTRIBUTIONS

D.T., J.W., X.Z., K.G., C.Q., and Z.Y. designed the experiments and analyzed the data. D.T., K.G., Z.Z., M.G., and Z.Y. cloned *Xa10*. D.T., X.Z., C.Q., and Z.Y. identified and characterized $EBE_{AvrXa10}$. D.T., X.Z., K.G., X.Y., J.W., and Z.Y. characterized XA10 function in plants. J.W., D.T., X.Y., M.M.-H., and Z.Y. investigated XA10-induced cell death in HeLa cells. F.F.W. contributed to the *Xa10* germplasm and AvrXa10 mutants. D.T., J.W., X.Z., K.G., F.F.W., and Z.Y. wrote the article. All authors read and approved the article.

Received October 6, 2013; revised December 30, 2013; accepted January 13, 2014; published January 31, 2014.

REFERENCES

Abas, L., and Luschnig, C. (2010). Maximum yields of microsomal-type membranes from small amounts of plant material without requiring ultracentrifugation. Anal. Biochem. **401:** 217–227.

Ali, R., Ma, W., Lemtiri-Chlieh, F., Tsaltas, D., Leng, Q., von Bodman, S., and Berkowitz, G.A. (2007). Death don't have no mercy and neither does calcium: *Arabidopsis* CYCLIC NUCLEOTIDE GATED CHANNEL2 and innate immunity. Plant Cell **19:** 1081–1095.

Antonsson, B., et al. (1997). Inhibition of Bax channel-forming activity by Bcl-2. Science **277:** 370–372.

Antony, G., Zhou, J., Huang, S., Li, T., Liu, B., White, F., and Yang, B. (2010). Rice xa13 recessive resistance to bacterial blight is defeated by induction of the disease susceptibility gene Os-11N3. Plant Cell **22:** 3864–3876.

Arabidopsis Genome Initiative (2000). Analysis of the genome sequence of the flowering plant *Arabidopsis thaliana*. Nature **408:** 796–815.

Ayliffe, M.A., Roberts, J.K., Mitchell, H.J., Zhang, R., Lawrence, G.J., Ellis, J.G., and Pryor, T.J. (2002). A plant gene up-regulated at rust infection sites. Plant Physiol. **129:** 169–180.

Ballvora, A., Pierre, M., van den Ackerveken, G., Schornack, S., Rossier, O., Ganal, M., Lahaye, T., and Bonas, U. (2001). Genetic mapping and functional analysis of the tomato *Bs4* locus governing recognition of the *Xanthomonas campestris* pv. *vesicatoria* AvrBs4 protein. Mol. Plant Microbe Interact. **14:** 629–638.

Boch, J., Scholze, H., Schornack, S., Landgraf, A., Hahn, S., Kay, S., Lahaye, T., Nickstadt, A., and Bonas, U. (2009). Breaking the code of DNA binding specificity of TAL-type III effectors. Science **326:** 1509–1512.

Bowling, S.A., Clarke, J.D., Liu, Y., Klessig, D.F., and Dong, X. (1997). The *cpr5* mutant of *Arabidopsis* expresses both NPR1-dependent and NPR1-independent resistance. Plant Cell **9:** 1573–1584.

Bradley, D.J., Kjellbom, P., and Lamb, C.J. (1992). Elicitor- and wound-induced oxidative cross-linking of a proline-rich plant cell wall protein: A novel, rapid defense response. Cell **70:** 21–30.

Chen, R., Valencia, I., Zhong, F., McColl, K.S., Roderick, H.L., Bootman, M.D., Berridge, M.J., Conway, S.J., Holmes, A.B., Mignery, G.A., Velez, P., and Distelhorst, C.W. (2004). Bcl-2 functionally interacts with inositol 1,4,5-trisphosphate receptors to regulate calcium release from the ER in response to inositol 1,4,5-trisphosphate. J. Cell Biol. **166:** 193–203.

Coll, N.S., Vercammen, D., Smidler, A., Clover, C., Van Breusegem, F., Dangl, J.L., and Epple, P. (2010). Arabidopsis type I metacaspases control cell death. Science **330:** 1393–1397.

del Pozo, O., and Lam, E. (1998). Caspases and programmed cell death in the hypersensitive response of plants to pathogens. Curr. Biol. **8:** 1129–1132.

Dyer, J.M., and Mullen, R.T. (2001). Immunocytological localization of two plant fatty acid desaturases in the endoplasmic reticulum. FEBS Lett. **494:** 44–47.

Feske, S., Gwack, Y., Prakriya, M., Srikanth, S., Puppel, S.-H., Tanasa, B., Hogan, P.G., Lewis, R.S., Daly, M., and Rao, A.

(2006). A mutation in Orai1 causes immune deficiency by abrogating CRAC channel function. Nature **441:** 179–185.

Görlach, A., Klappa, P., and Kietzmann, T. (2006). The endoplasmic reticulum: Folding, calcium homeostasis, signaling, and redox control. Antioxid. Redox Signal. **8:** 1391–1418.

Grant, M., Brown, I., Adams, S., Knight, M., Ainslie, A., and Mansfield, J. (2000). The RPM1 plant disease resistance gene facilitates a rapid and sustained increase in cytosolic calcium that is necessary for the oxidative burst and hypersensitive cell death. Plant J. **23:** 441–450.

Gu, K., Chiam, H., Tian, D., and Yin, Z. (2011). Molecular cloning and expression of heteromeric ACCase subunit genes from Jatropha curcas. Plant Sci. **180:** 642–649.

Gu, K., Sangha, J.S., Li, Y., and Yin, Z. (2008). High-resolution genetic mapping of bacterial blight resistance gene *Xa10*. Theor. Appl. Genet. **116:** 155–163.

Gu, K., Tian, D., Qiu, C., and Yin, Z. (2009). Transcription activator-like type III effector AvrXa27 depends on OsTFIIAgamma5 for the activation of *Xa27* transcription in rice that triggers disease resistance to *Xanthomonas oryzae* pv. *oryzae*. Mol. Plant Pathol. **10:** 829–835.

Gu, K., Tian, D., Yang, F., Wu, L., Sreekala, C., Wang, D., Wang, G.L., and Yin, Z. (2004). High-resolution genetic mapping of *Xa27 (t)*, a new bacterial blight resistance gene in rice, *Oryza sativa* L. Theor. Appl. Genet. **108:** 800–807.

Gu, K., Yang, B., Tian, D., Wu, L., Wang, D., Sreekala, C., Yang, F., Chu, Z., Wang, G.L., White, F.F., and Yin, Z. (2005). *R* gene expression induced by a type-III effector triggers disease resistance in rice. Nature **435:** 1122–1125.

Haseloff, J., Siemering, K.R., Prasher, D.C., and Hodge, S. (1997). Removal of a cryptic intron and subcellular localization of green fluorescent protein are required to mark transgenic Arabidopsis plants brightly. Proc. Natl. Acad. Sci. USA **94:** 2122–2127.

He, S., Wang, L., Miao, L., Wang, T., Du, F., Zhao, L., and Wang, X. (2009). Receptor interacting protein kinase-3 determines cellular necrotic response to TNF-α. Cell **137:** 1100–1111.

Heath, M.C. (2000). Hypersensitive response-related death. Plant Mol. Biol. **44:** 321–334.

Hiei, Y., Ohta, S., Komari, T., and Kumashiro, T. (1994). Efficient transformation of rice (*Oryza sativa* L.) mediated by *Agrobacterium* and sequence analysis of the boundaries of the T-DNA. Plant J. **6:** 271–282.

Hopkins, C.M., White, F.F., Choi, S.H., Guo, A., and Leach, J.E. (1992). Identification of a family of avirulence genes from *Xanthomonas oryzae* pv. *oryzae*. Mol. Plant Microbe Interact. **5:** 451–459.

Hou, X., Pedi, L., Diver, M.M., and Long, S.B. (2012). Crystal structure of the calcium release-activated calcium channel Orai. Science **338:** 1308–1313.

Iwano, M., Entani, T., Shiba, H., Kakita, M., Nagai, T., Mizuno, H., Miyawaki, A., Shoji, T., Kubo, K., Isogai, A., and Takayama, S. (2009). Fine-tuning of the cytoplasmic Ca^{2+} concentration is essential for pollen tube growth. Plant Physiol. **150:** 1322–1334.

Iyer, A.S., and McCouch, S.R. (2004). The rice bacterial blight resistance gene *xa5* encodes a novel form of disease resistance. Mol. Plant Microbe Interact. **17:** 1348–1354.

Jabs, T., Tschöpe, M., Colling, C., Hahlbrock, K., and Scheel, D. (1997). Elicitor-stimulated ion fluxes and O2- from the oxidative burst are essential components in triggering defense gene activation and phytoalexin synthesis in parsley. Proc. Natl. Acad. Sci. USA **94:** 4800–4805.

Kadota, Y., Furuichi, T., Ogasawara, Y., Goh, T., Higashi, K., Muto, S., and Kuchitsu, K. (2004). Identification of putative voltage-dependent Ca^{2+}-permeable channels involved in cryptogein-induced Ca^{2+} transients and defense responses in tobacco BY-2 cells. Biochem. Biophys. Res. Commun. **317:** 823–830.

Kawai-Yamada, M., Jin, L., Yoshinaga, K., Hirata, A., and Uchimiya, H. (2001). Mammalian Bax-induced plant cell death can be down-regulated by overexpression of Arabidopsis Bax Inhibitor-1 (AtBI-1). Proc. Natl. Acad. Sci. USA **98:** 12295–12300.

Kay, S., Hahn, S., Marois, E., Hause, G., and Bonas, U. (2007). A bacterial effector acts as a plant transcription factor and induces a cell size regulator. Science **318:** 648–651.

Krysko, D.V., Vanden Berghe, T., D'Herde, K., and Vandenabeele, P. (2008). Apoptosis and necrosis: Detection, discrimination and phagocytosis. Methods **44:** 205–221.

Kurusu, T., Sakurai, Y., Miyao, A., Hirochika, H., and Kuchitsu, K. (2004). Identification of a putative voltage-gated Ca^{2+}-permeable channel (OsTPC1) involved in Ca^{2+} influx and regulation of growth and development in rice. Plant Cell Physiol. **45:** 693–702.

Lacomme, C., and Santa Cruz, S. (1999). Bax-induced cell death in tobacco is similar to the hypersensitive response. Proc. Natl. Acad. Sci. USA **96:** 7956–7961.

Lecourieux, D., Ranjeva, R., and Pugin, A. (2006). Calcium in plant defence-signalling pathways. New Phytol. **171:** 249–269.

Leng, Q., Mercier, R.W., Yao, W., and Berkowitz, G.A. (1999). Cloning and first functional characterization of a plant cyclic nucleotide-gated cation channel. Plant Physiol. **121:** 753–761.

Levine, A., Tenhaken, R., Dixon, R., and Lamb, C. (1994). H_2O_2 from the oxidative burst orchestrates the plant hypersensitive disease resistance response. Cell **79:** 583–593.

Li, P., Nijhawan, D., Budihardjo, I., Srinivasula, S.M., Ahmad, M., Alnemri, E.S., and Wang, X. (1997). Cytochrome c and dATP-dependent formation of Apaf-1/caspase-9 complex initiates an apoptotic protease cascade. Cell **91:** 479–489.

Liu, X., Kim, C.N., Yang, J., Jemmerson, R., and Wang, X. (1996). Induction of apoptotic program in cell-free extracts: requirement for dATP and cytochrome c. Cell **86:** 147–157.

Liu, Y., Ren, D., Pike, S., Pallardy, S., Gassmann, W., and Zhang, S. (2007). Chloroplast-generated reactive oxygen species are involved in hypersensitive response-like cell death mediated by a mitogen-activated protein kinase cascade. Plant J. **51:** 941–954.

Liu, Y., Schiff, M., Czymmek, K., Tallóczy, Z., Levine, B., and Dinesh-Kumar, S.P. (2005). Autophagy regulates programmed cell death during the plant innate immune response. Cell **121:** 567–577.

Luo, X., He, Q., Huang, Y., and Sheikh, M.S. (2005). Transcriptional upregulation of PUMA modulates endoplasmic reticulum calcium pool depletion-induced apoptosis via Bax activation. Cell Death Differ. **12:** 1310–1318.

Ma, W., Ali, R., and Berkowitz, G.A. (2006). Characterization of plant phenotypes associated with loss-of-function of AtCNGC1, a plant cyclic nucleotide gated cation channel. Plant Physiol. Biochem. **44:** 494–505.

Ma, W., and Berkowitz, G.A. (2007). The grateful dead: Calcium and cell death in plant innate immunity. Cell. Microbiol. **9:** 2571–2585.

Mathai, J.P., Germain, M., and Shore, G.C. (2005). BH3-only BIK regulates BAX,BAK-dependent release of Ca^{2+} from endoplasmic reticulum stores and mitochondrial apoptosis during stress-induced cell death. J. Biol. Chem. **280:** 23829–23836.

Montillet, J.-L., Chamnongpol, S., Rustérucci, C., Dat, J., van de Cotte, B., Agnel, J.-P., Battesti, C., Inzé, D., Van Breusegem, F., and Triantaphylidès, C. (2005). Fatty acid hydroperoxides and H_2O_2 in the execution of hypersensitive cell death in tobacco leaves. Plant Physiol. **138:** 1516–1526.

Moscou, M.J., and Bogdanove, A.J. (2009). A simple cipher governs DNA recognition by TAL effectors. Science **326:** 1501.

Palmer, A.E., Jin, C., Reed, J.C., and Tsien, R.Y. (2004). Bcl-2-mediated alterations in endoplasmic reticulum Ca^{2+} analyzed with an improved genetically encoded fluorescent sensor. Proc. Natl. Acad. Sci. USA **101:** 17404–17409.

Palmer, A.E., and Tsien, R.Y. (2006). Measuring calcium signaling using genetically targetable fluorescent indicators. Nat. Protoc. **1:** 1057–1065.

Parker, M., Pattus, F., Tucker, A., and Tsernoglou, D. (1989). Structure of the membrane-pore-forming fragment of colicin A. Nature. **337:** 93–96.

Peiter, E., Maathuis, F.J., Mills, L.N., Knight, H., Pelloux, J., Hetherington, A.M., and Sanders, D. (2005). The vacuolar Ca^{2+}-activated channel TPC1 regulates germination and stomatal movement. Nature **434:** 404–408.

Petros, A.M., Olejniczak, E.T., and Fesik, S.W. (2004). Structural biology of the Bcl-2 family of proteins. Biochim. Biophys. Acta Mol. Cell Res. **1644:** 83–94.

Pinton, P., Giorgi, C., Siviero, R., Zecchini, E., and Rizzuto, R. (2008). Calcium and apoptosis: ER-mitochondria Ca^{2+} transfer in the control of apoptosis. Oncogene **27:** 6407–6418.

Prakriya, M., Feske, S., Gwack, Y., Srikanth, S., Rao, A., and Hogan, P.G. (2006). Orai1 is an essential pore subunit of the CRAC channel. Nature **443:** 230–233.

Qi, Z., Stephens, N.R., and Spalding, E.P. (2006). Calcium entry mediated by GLR3.3, an Arabidopsis glutamate receptor with a broad agonist profile. Plant Physiol. **142:** 963–971.

Rizzuto, R., Pinton, P., Carrington, W., Fay, F.S., Fogarty, K.E., Lifshitz, L.M., Tuft, R.A., and Pozzan, T. (1998). Close contacts with the endoplasmic reticulum as determinants of mitochondrial Ca^{2+} responses. Science **280:** 1763–1766.

Rojo, E., Martín, R., Carter, C., Zouhar, J., Pan, S., Plotnikova, J., Jin, H., Paneque, M., Sánchez-Serrano, J.J., Baker, B., Ausubel, F.M., and Raikhel, N.V. (2004). VPEgamma exhibits a caspase-like activity that contributes to defense against pathogens. Curr. Biol. **14:** 1897–1906.

Römer, P., Hahn, S., Jordan, T., Strauss, T., Bonas, U., and Lahaye, T. (2007). Plant pathogen recognition mediated by promoter activation of the pepper *Bs3* resistance gene. Science **318:** 645–648.

Römer, P., Recht, S., and Lahaye, T. (2009). A single plant resistance gene promoter engineered to recognize multiple TAL effectors from disparate pathogens. Proc. Natl. Acad. Sci. USA **106:** 20526–20531.

Schlesinger, P.H., Gross, A., Yin, X.-M., Yamamoto, K., Saito, M., Waksman, G., and Korsmeyer, S.J. (1997). Comparison of the ion channel characteristics of proapoptotic BAX and antiapoptotic BCL-2. Proc. Natl. Acad. Sci. USA **94:** 11357–11362.

Schornack, S., Ballvora, A., Gürlebeck, D., Peart, J., Baulcombe, D., Ganal, M., Baker, B., Bonas, U., and Lahaye, T. (2004). The tomato resistance protein Bs4 is a predicted non-nuclear TIR-NB-LRR protein that mediates defense responses to severely truncated derivatives of AvrBs4 and overexpressed AvrBs3. Plant J. **37:** 46–60.

Scorrano, L., Oakes, S.A., Opferman, J.T., Cheng, E.H., Sorcinelli, M. D., Pozzan, T., and Korsmeyer, S.J. (2003). BAX and BAK regulation of endoplasmic reticulum Ca^{2+}: A control point for apoptosis. Science **300:** 135–139.

Shockey, J.M., Gidda, S.K., Chapital, D.C., Kuan, J.-C., Dhanoa, P.K., Bland, J.M., Rothstein, S.J., Mullen, R.T., and Dyer, J.M. (2006). Tung tree DGAT1 and DGAT2 have nonredundant functions in triacylglycerol biosynthesis and are localized to different subdomains of the endoplasmic reticulum. Plant Cell **18:** 2294–2313.

Shore, G.C., Papa, F.R., and Oakes, S.A. (2011). Signaling cell death from the endoplasmic reticulum stress response. Curr. Opin. Cell Biol. **23:** 143–149.

Strauss, T., et al. (2012). RNA-seq pinpoints a Xanthomonas TAL-effector activated resistance gene in a large-crop genome. Proc. Natl. Acad. Sci. USA **109:** 19480–19485.

Sugio, A., Yang, B., Zhu, T., and White, F.F. (2007). Two type III effector genes of *Xanthomonas oryzae* pv. *oryzae* control the induction of the host genes OsTFIIAgamma1 and OsTFX1 during bacterial blight of rice. Proc. Natl. Acad. Sci. USA **104:** 10720–10725.

Thordal-Christensen, H., Zhang, Z., Wei, Y., and Collinge, D.B. (1997). Subcellular localization of H_2O_2 in plants. H_2O_2 accumulation in papillae and hypersensitive response during the barley–powdery mildew interaction. Plant J. **11:** 1187–1194.

Wittig, I., Braun, H.-P., and Schägger, H. (2006). Blue native PAGE. Nat. Protoc. **1:** 418–428.

Yang, B., Sugio, A., and White, F.F. (2006). *Os8N3* is a host disease-susceptibility gene for bacterial blight of rice. Proc. Natl. Acad. Sci. USA **103:** 10503–10508.

Yang, B., and White, F.F. (2004). Diverse members of the AvrBs3/PthA family of type III effectors are major virulence determinants in bacterial blight disease of rice. Mol. Plant Microbe Interact. **17:** 1192–1200.

Yoshimura, A., Mew, T., Khush, G., and Omura, T. (1983). Inheritance of resistance to bacterial blight in rice cultivar Cas 209. Phytopathology **73:** 1409–1412.

Yue, J.X., Meyers, B.C., Chen, J.Q., Tian, D., and Yang, S. (2012). Tracing the origin and evolutionary history of plant nucleotide-binding site-leucine-rich repeat (NBS-LRR) genes. New Phytol. **193:** 1049–1063.

Zhang, Y., Su, J., Duan, S., Ao, Y., Dai, J., Liu, J., Wang, P., Li, Y., Liu, B., Feng, D., Wang, J., and Wang, H. (2011). A highly efficient rice green tissue protoplast system for transient gene expression and studying light/chloroplast-related processes. Plant Methods **7:** 30.

Zhu, W., Yang, B., Chittoor, J.M., Johnson, L.B., and White, F.F. (1998). AvrXa10 contains an acidic transcriptional activation domain in the functionally conserved C terminus. Mol. Plant Microbe Interact. **11:** 824–832.

Zurbriggen, M.D., Carrillo, N., Tognetti, V.B., Melzer, M., Peisker, M., Hause, B., and Hajirezaei, M.R. (2009). Chloroplast-generated reactive oxygen species play a major role in localized cell death during the non-host interaction between tobacco and *Xanthomonas campestris* pv. *vesicatoria*. Plant J. **60:** 962–973.